TECHNICAL REPORT ECOM-01362-F

STUDY AND INVESTIGATION LEADING TO THE DESIGN OF BROADBAND HIGH POWER KLYSTRON AMPLIFIERS

Final Report

By

ERLING LIEN - DARRELL ROBINSON

NOVEMBER, 1966

ECOM

UNITED STATES ARMY ELECTRONICS COMMAND • FORT MONMOUTH, N.J. 07703

CONTRACT DA 28-043 AMC 01362(E)

EIMAC

DIVISION OF VARIAN

301 Industrial Way

San Carlos, California

NOTICES

DISCLAIMERS

The findings in this report are not to be construed as an official Department of the Army position, unless so designated by other authorized documents.

The citation of trade names and names of manufacturers in this report is not to be construed as official Government indorsement or approval of commercial products or services referenced herein.

DISPOSITION

Destroy this report when it is no longer needed. Do not return it to the originator.

TECHNICAL REPORT ECOM-01362-F November, 1966

STUDY AND INVESTIGATION LEADING to the DESIGN OF BROADBAND HIGH POWER KLYSTRON AMPLIFIERS

FINAL REPORT

March 1, 1966 through August 31, 1966

Report No. 4

Prepared by

E. Lien and D. Robinson

EIMAC, A Division of Varian Associates

San Carlos, California

CON. NO. DA 28-043 AMC 01362(E)

DA PROJ. NO. 5624-11-905-04-78

For

UNITED STATES ARMY ELECTRONICS COMMAND

Fort Monmouth, New Jersey 07703

ABSTRACT

The objective of this program has been to investigate rf interaction circuits and stagger-tuning techniques leading to at least a fifty percent improvement in the 1 db bandwidth of high-power klystrons over the current state-of-the-art.

In this report, the findings of the final phase of this contract are presented. The major part of the effort during this final reporting period included: the completion of large-signal efficiency calculations across the band assuming a filter-loaded output resonator, the final theoretical design of the buncher section, theoretical stability calculations on the filter-loaded output resonator, and cold test measurements on a filter-loaded extended-interaction resonator.

The measured interaction impedance obtained with the cold-test filter-loaded output resonator closely approximated the impedance assumed in the theoretical efficiency calculations. The final buncher section, designed with the aid of the small-signal computer program, yielded a nearly constant rf drive current to the output resonator, as was assumed in the large-signal efficiency calculations. The small-signal analysis indicated that conventional single-gap resonators are to be preferred over extended-interaction resonators in the klystron buncher section at the high power level considered in this study.

The combined results of the small-signal analyses, the large-signal analyses, and the cold test measurements carried out during this contract show the feasibility of building a 5 megawatt peak-power C-band klystron

ABSTRACT (Continued)

amplifier with a 14 percent 1 db bandwidth, with a predicted efficiency of nearly 50 percent, and with a predicted gain of more than 30 db. The only element of the final klystron model which is not conventionally found in klystron amplifiers is the filter-loaded two-gap extended-interaction output resonator.

FOREWORD

This document is a report of the work performed on Contract DA 28-043 AMC-01362(E) during the final period.

The program was carried out in the High Power Microwave Tube Laboratory. The principal engineers were Erling Lien, who served as project leader, and Darrell Robinson. Another major contributor during the final period was Marta Perry (mathematician).

Sponsorship and direction of the program were from the U.S. Army Electronics Command, Fort Monmouth, New Jersey. The assigned Army Project Engineer was Park Richmond.

TABLE OF CONTENTS

TABLE OF CONTENTS (Continued)

LIST OF FIGURES

LIST OF FIGURES (Continued)

I. INTRODUCTION

The objective of this program has been to investigate rf interaction circuits and stagger-tuning techniques leading to at least a fifty percent improvement in the 1 db bandwidth of high-power klystrons over the current state-of-the-art. The possible methods by which this objective might be met were studied both theoretically and with cold testing. The cold test measurements provided a basis for the values of the parameters used in the latest theoretical calculations.

A design example of a 5 megawatt C-band klystron was chosen for the investigation. Design goals for this tube included a 14 percent 1 db bandwidth, a minimum saturated gain of 35 db, and a minimum efficiency of 35 percent. All tube parameters were chosen to be consistent with present day tube techniques. The values of the klystron parameters originally chosen for the calculations were listed in Section I of the First Quarterly Report. These parameters were altered only slightly during the course of the contract (See Section III, Part B of this report for the two changes that were made).

The study of the example klystron was divided into two general areas: the buncher section and the output resonator. Considered for use in the buncher section were conventional single-gap resonators, and two-gap π-mode and 2π-mode extended interaction resonators. Candidates for the output resonator included the conventional resonators, the two-gap extended-interaction resonators, and filter-loaded versions of these same types. By the end of the previous quarter the choice of buncher resonators had been

narrowed to either conventional single-gap resonators or π-mode extended-interaction resonators. A two-gap π-mode resonator with single-section filter loading was selected for the klystron output. The reasons for these choices were given in the preceding quarterly reports.

During the present reporting period, large-signal efficiency calculations were completed on a π-mode filter-loaded output resonator at a number of frequencies across the band. Once the large-signal analysis was complete, showing that the rf current from the buncher section should be nearly constant with frequency, the design of the buncher section was finalized. The characteristics of the filter-loaded resonator were studied in more detail both theoretically and in cold test. The theoretical study was concerned primarily with the resonator stability. The progress in each area of investigation is discussed in the sections following. At the end of the report some conclusions are drawn from the findings of this contract, and recommendations for future work are presented.

II. LARGE-SIGNAL ANALYSIS OF THE OUTPUT REGION

A. Introduction

During the previous quarter, a number of different types of output resonators were analyzed for their large-signal performance at the center of the band. These included single-gap resonators and two-gap extended-interaction resonators operating in either the π mode or the 2π mode. It was seen that a π-mode resonator with a normalized gap-to-gap spacing of approximately 2.2 radians gave the best results at the loading required to yield a 14 percent 1 db bandwidth. It was further shown that the addition of a single-section filter to the output resonator substantially raised its interaction impedance and also the output efficiency.

During the period covered by this report, the investigation of the large-signal behavior of the klystron has been extended to cover the entire operating frequency band. In view of the results from the previous quarter, the output resonator chosen for the klystron model was a two-gap π-mode extended-interaction resonator with single-section filter loading. Its large-signal operation was studied at five different frequencies: the center of the band, at the two band edges (where both the frequency and the resonator impedance phase angle have their extreme values), and at the two frequencies where the real part of the resonator impedance is a maximum. The details of this analysis and the results are discussed in this section.

B. RF Beam Current from the Buncher Section

It was shown in the Third Quarterly Report that the equation used to compute the output conversion efficiency in the large-signal computer program can be written in the following form:

$$\eta_c = \frac{1}{2}\frac{|Z|}{Z_o}\left(\frac{|I_\infty|}{I_o}\right)^2 \cos\phi = \frac{1}{2}\left(\frac{|I_\infty|}{I_o}\right)^2 \frac{Re\,(Z)}{Z_o} \qquad (1)$$

where:

$\frac{|I_\infty|}{I_o}$ = normalized induced current magnitude in the output resonator

Z_o = dc beam impedance

Z = output resonator interaction impedance

$Re\,(Z)$ = real part of Z

ϕ = output resonator impedance phase angle

In order for the output power variation to be less than 1 db across the band, the output resonator impedance and the rf current driving the resonator must be tailored until

$$\frac{\eta_c}{(\eta_c)_{max}} \geq 0.794 \qquad (2)$$

Initially, it was assumed that the best way to achieve this goal would be to have an output resonator whose impedance was symmetrical about the center of the band, and to have the induced rf

current in that resonator as constant as possible at each frequency. It was further assumed that the induced current would be nearly constant if the rf current driving the resonator was constant. (It was expected that there would be some change in the current induced at different frequencies by a constant drive current due to changes in the beam remodulation within the output resonator. That this is true will be shown later.) Accordingly, at each frequency where the large-signal behavior of the buncher was studied, the voltage on the prepenultimate resonator (the first resonator analyzed) was adjusted until the signal level at the position of the output resonator simulated saturation conditions, and the value of the rf beam current at that location was essentially constant. In each case, the voltages on the penultimate resonators were chosen to make the resulting penultimate impedances consistent with the assumed operating frequency and resonator detuning. Curves have already been presented in previous reports showing the fundamental component of the rf beam current in the output region of the tube at the band center and at the band edges. The curves for the other two frequencies investigated are similar. The results for all five frequencies are summarized in Table I below. $|I_1|/I_o$ is the normalized fundamental component of the rf current from the buncher at the center of the output resonator. The values of α_1 and α_2 are the normalized rf voltages on the two gaps of the extended-interaction prepenultimate resonator; α_3 and α_4 are the voltages on the penultimate resonator gaps.

TABLE I

Normalized Frequency ω/ω_o	$\frac{\lvert I_1 \rvert}{I_o}$	$\alpha_1=\alpha_2$	α_3	α_4
0.93	1.42	.20	.173	.226
0.95	1.39	.185	.175	.234
1.0	1.41	.15	.21	.30
1.05	1.46	.095	.257	.446
1.07	1.47	.07	.276	.565

As seen, the rf drive $|I_1|/I_o$ is approximately constant over the band.

It should be noted that at each new frequency, all tube parameters which are normalized to frequency were adjusted. The corrections involved the normalized gap parameters, normalized axial distance, and the space-charge wave reduction factor.

C. Output Resonator Model

The results presented in Sections IV and V of the Third Quarterly Report indicated that, from an efficiency standpoint, the best output resonator for the tube model under study is a π-mode extended-interaction resonator with filter loading. This is the type of resonator which has been assumed in the large-signal calculations across the band. (We have restricted the number of gaps in the extended-interaction resonator to two, and have considered only single-section filters in our study.) The normalized gap-to-gap spacing chosen for the

two-gap resonator was 2.2 radians, which is near the optimum value at the loading required to achieve a 14 percent 1 db bandwidth.

For the purpose of finding the resonator impedance as a function of frequency, we have chosen to represent the two-gap filter-loaded structure by the same two-mesh equivalent circuit that was used in the earlier analysis of double-tuned buncher resonators (See Fig. 7 of the Second Quarterly Report). The two-gap resonator is assumed to be replaced by a single circuit whose frequency, Q, and R/Q are equal to the respective quantities of the overall two-gap resonator in the π mode. The second mesh of the equivalent circuit represents the filter cavity. It is felt that the single-mesh representation of the two-gap resonator is valid as long as the separation between the two resonator modes is sufficient to assure negligible excitation of the non-operating mode. (This condition is satisfied in the cold test structures on which measurements have been made.) As a check on the validity of this assumption, the resonator impedance predicted by the two-mesh circuit was compared with the impedance predicted by the more exact three-mesh equivalent circuit being used in the investigation of resonator stability (See Section IV of this report). The agreement was good.

For the calculation of the large-signal behavior of the output resonator, its axial electric field was assumed to be a single-period sinusoidal field. (The large-signal program at present allows only constant, sinusoidal, or cosinusoidal gap fields. To use the actual gap field in the calculations would require a major modification of

the program.) This assumed field model has been compared with the actual field on the axis of the resonator (obtained by perturbation methods). The two fields are almost identical except near the ends of the resonator, where tha actual field tapers off more gradually than the sinusoidal field. Calculations performed to evaluate the effect of this difference indicate that the efficiency obtained with the real resonator may be from one to four percent lower than the efficiencies computed with the sinusoidal field.

D. Output Efficiency Across the Band

The rf beam current obtained from the large-signal analysis of the buncher section, summarized in Table I, was used to drive a two-gap π-mode filter-loaded output resonator. Some of the general aspects of the output resonator model have been described above. The particular impedance vs. frequency curve assumed in the calculations is shown in Figs. 1, 2, and 3 in which the real part, magnitude, and phase angle of the impedance are plotted, respectively. The resonator parameters are listed on the figures. As before, the subscript 1 refers to the resonator coupled to the beam while the subscript 2 refers to the filter cavity.

The resulting output conversion efficiency computed at each frequency is listed in Table II.

The values of normalized efficiency from the table are plotted vs. frequency in Fig. 4. For comparison, the real part of the resonator interaction impedance, normalized to the maximum-value, is also plotted in the figure.

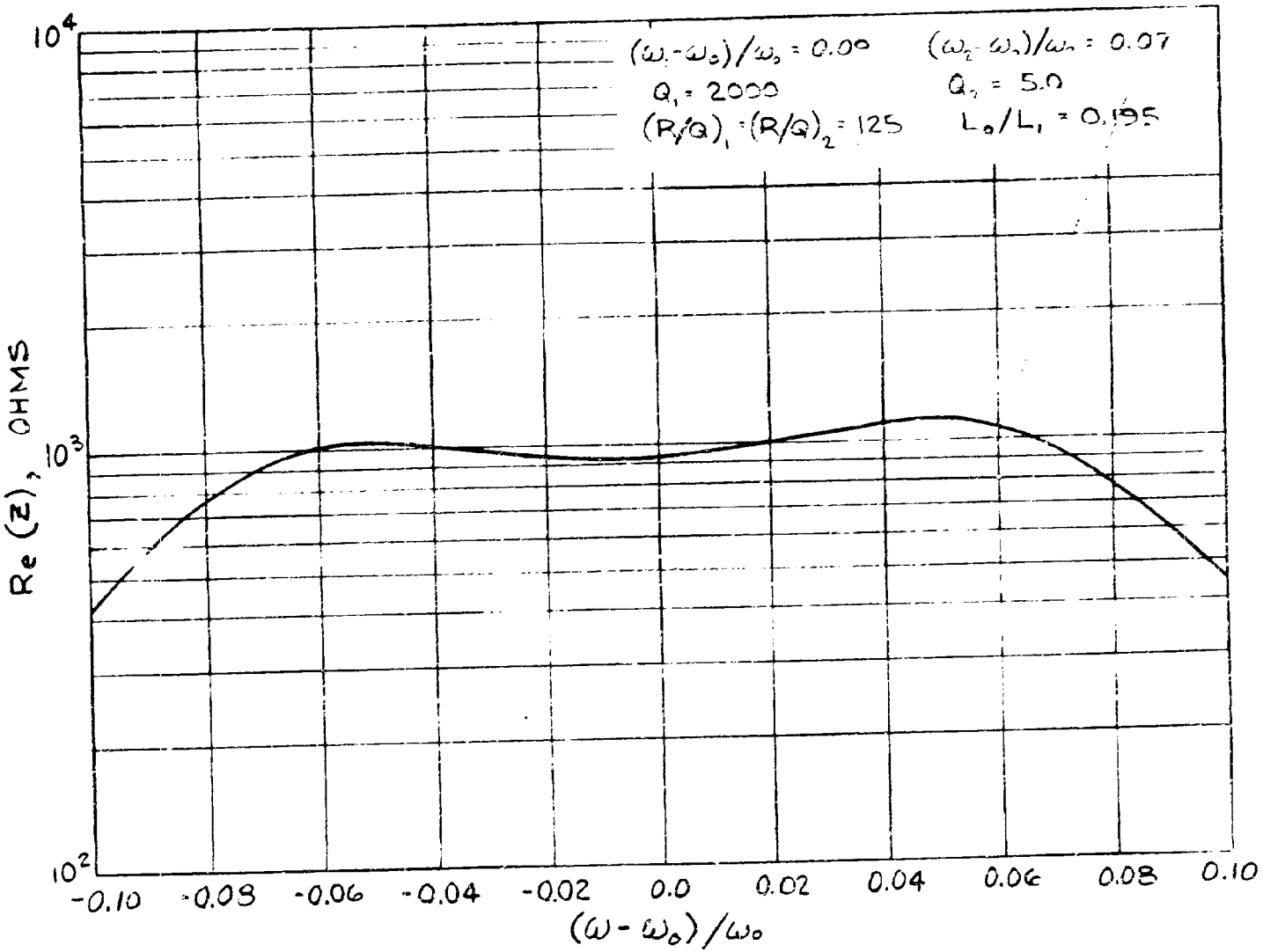

Fig. 1 - Real part of the interaction impedance of a filter-loaded output resonator (theoretical).

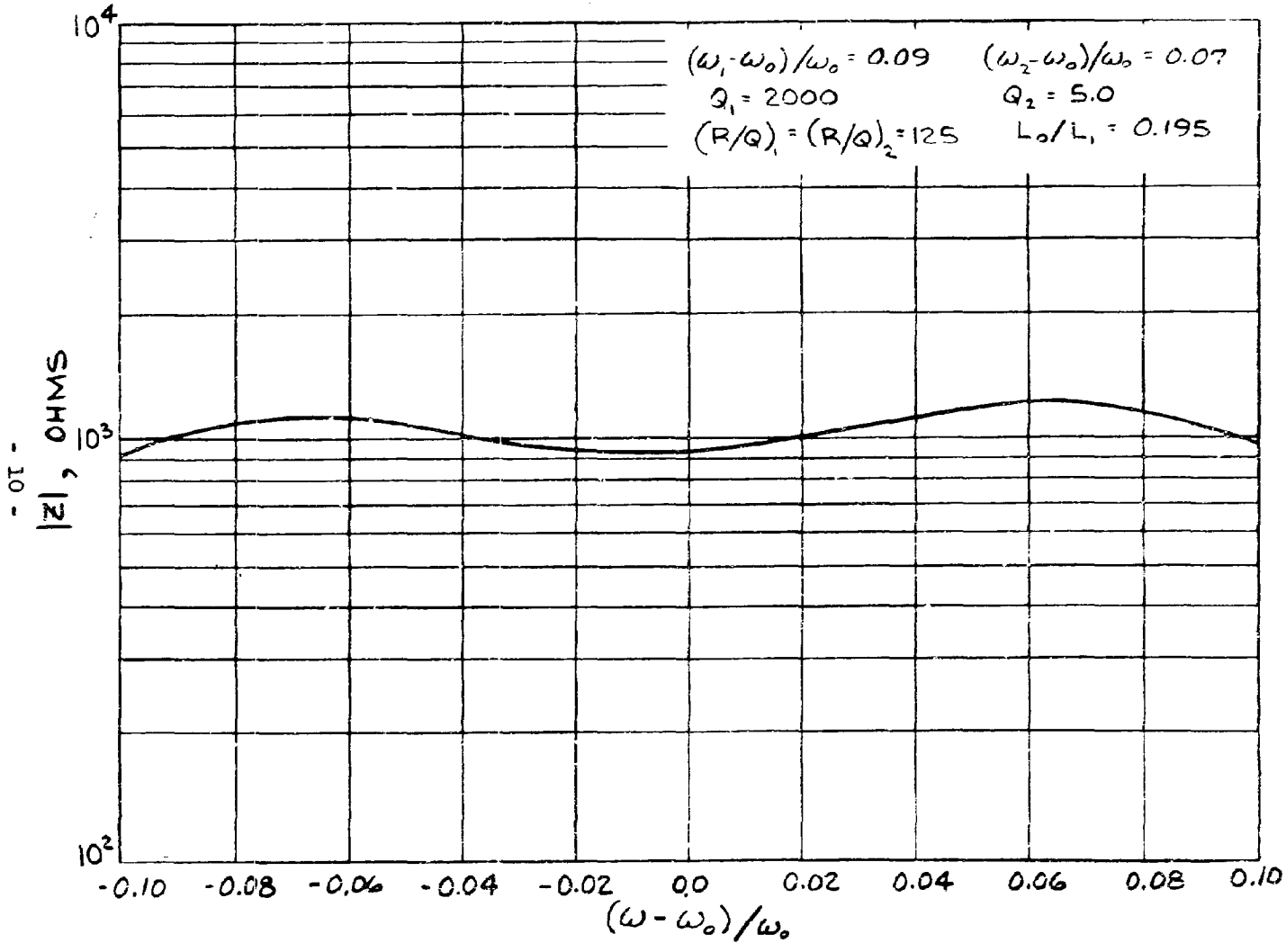

Fig. 2 - Filter-loaded output resonator interaction impedance magnitude (theoretical).

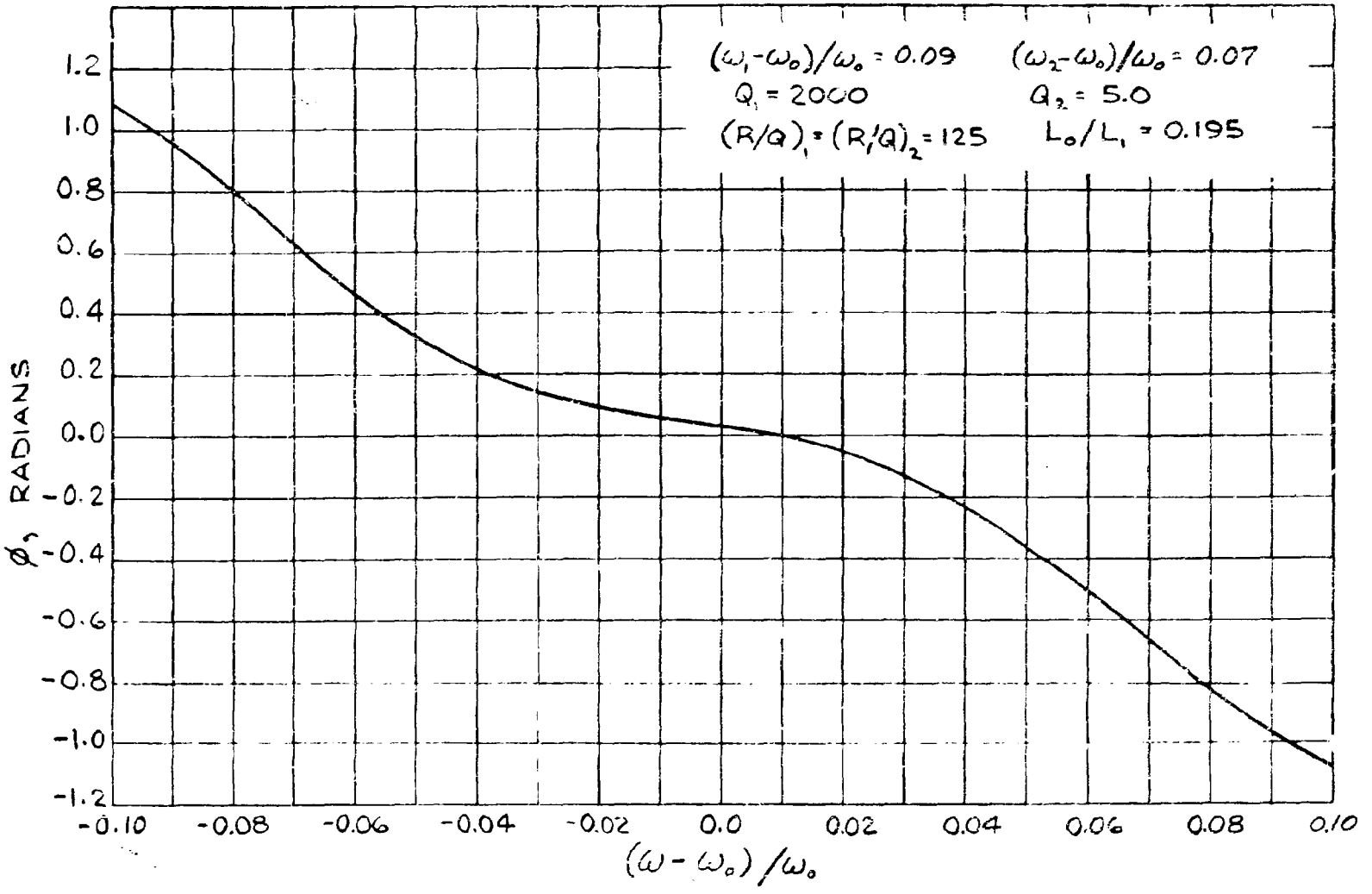

Fig. 3 - Filter-loaded output resonator interaction impedance phase angle (theoretical).

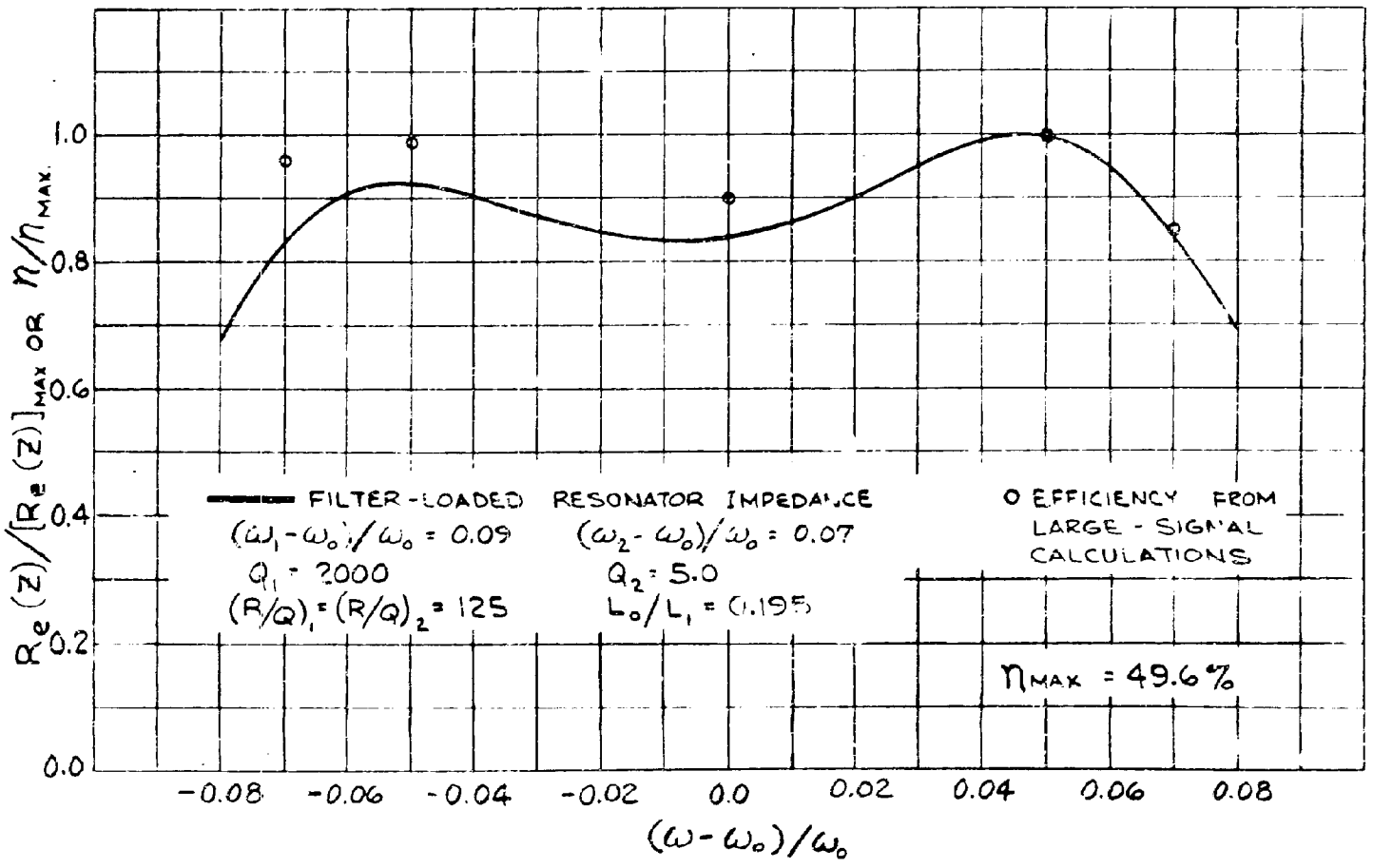

Fig. 4 - Calculated efficiency variation across the band compared with the variation of the real part of the output resonator interaction impedance.

TABLE II

Normalized Frequency ω/ω_o	Efficiency, η	$\frac{\eta}{\eta_{max}}$
0.93	47.5%	.96
0.95	49.2%	.99
1.00	44.8%	.90
1.05	49.6%	1.00
1.07	42.1%	.85

Since the frequencies at which the efficiency was computed represent the extreme points of both the real part of the impedance and the impedance phase angle, it is expected that the efficiency at frequencies between the points of calculation will lie on a smooth curve between the points. Thus, with constant beam power, the variation of the rf output power will be less than 1 db across the entire band for the case illustrated. The results presented here demonstrate the feasibility of obtaining a 14 percent 1 db bandwidth at a good efficiency level. This feasibility is, of course, contingent on the ability to obtain a constant rf drive current from the buncher across the band and an output resonator interaction impedance curve similar to the one assumed. These latter considerations will be discussed more in the sections to follow.

Referring to Fig. 4, the fact that the points of normalized efficiency lie above the curve of normalized impedance at the low end of the band, whereas the rf drive current to the output resonator

is actually lower at that end of the band, is an indication of the decrease in the beam remodulation within the output resonator as the frequency increases. The quantitative aspects of this phenomenon are illustrated graphically in Figs. 5, 6, and 7. The normalized fundamental rf beam current is plotted as a function of normalized distance at three different frequencies. The dashed curves show the rf current from the buncher section with zero voltage on the output resonator; the solid curves show the current with the output resonator present. It is seen that there is a considerable remodulation of the beam at the low end of the band, a small amount of remodulation at the center of the band, and a net demodulation of the beam at the high end of the band. This general behavior was anticipated from the small-signal analysis of extended-interaction resonators, but the actual magnitude of the change in the beam remodulation with frequency was not known until the large-signal calculations had been performed.

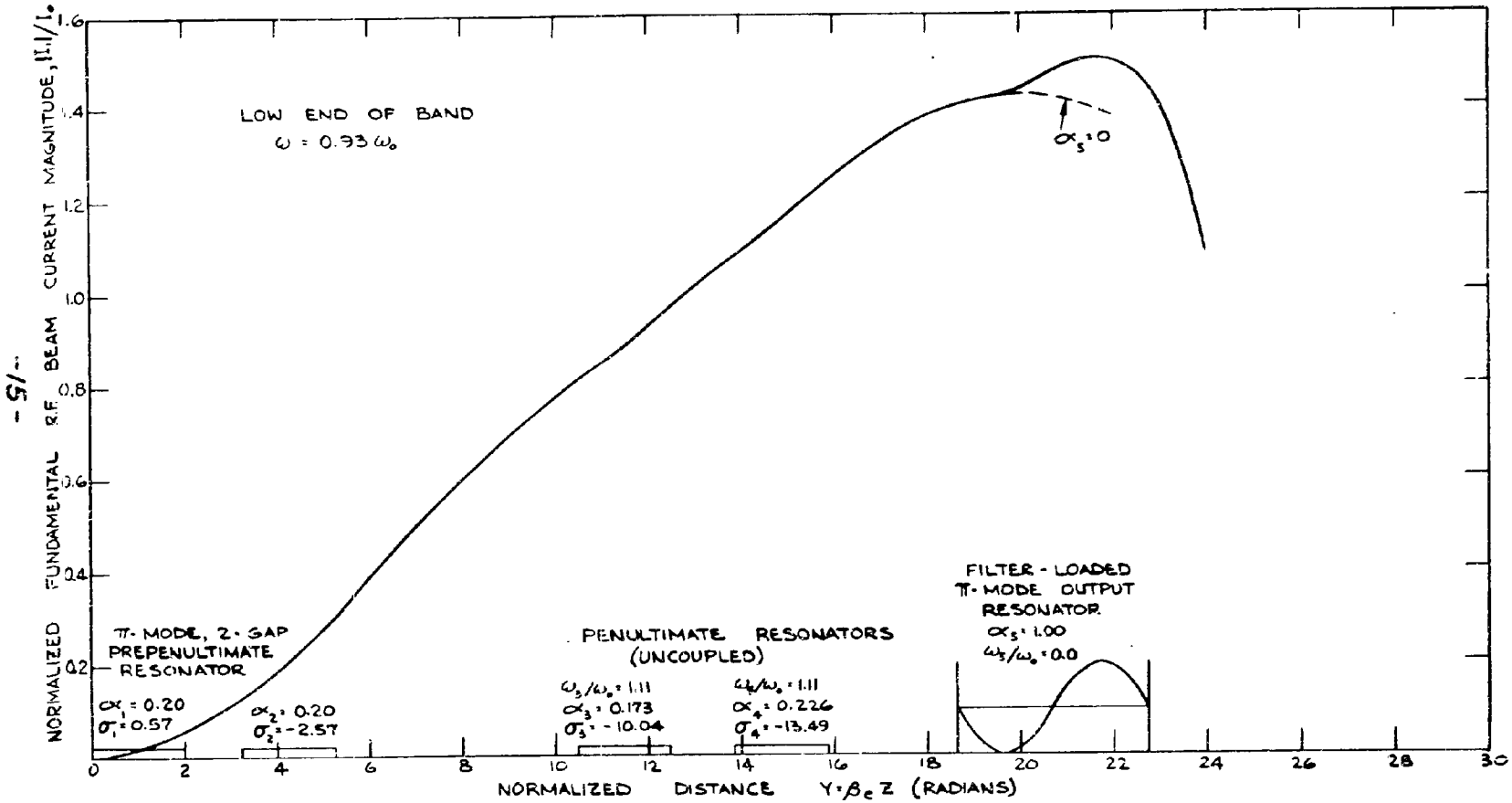

FIG 5 FUNDAMENTAL RF BEAM CURRENT VS. DISTANCE IN THE KLYSTRON OUTPUT REGION AT LOWER BAND EDGE.

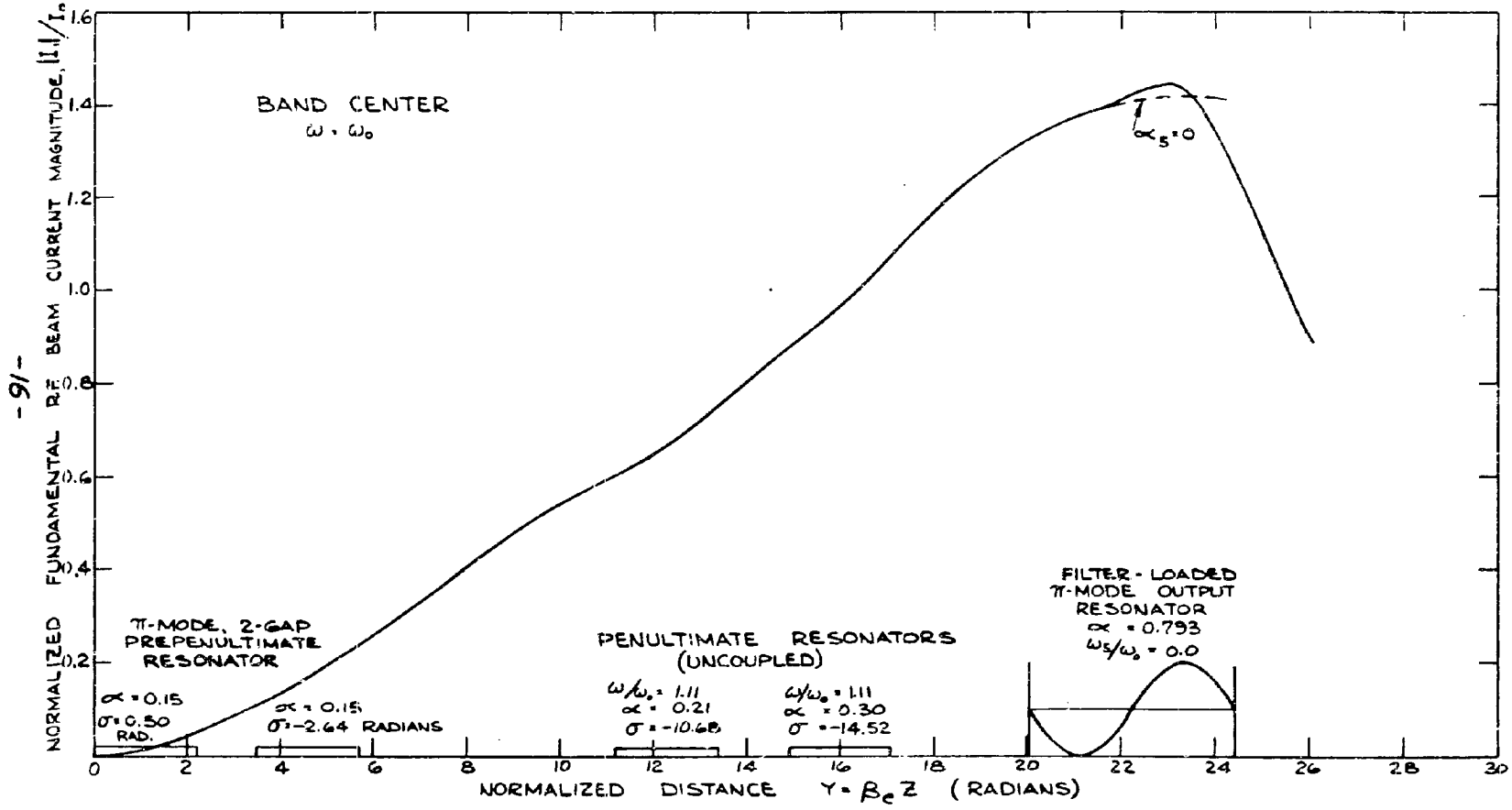

FIG. 6 FUNDAMENTAL RF BEAM CURRENT VS DISTANCE IN THE KLYSTRON OUTPUT REGION AT THE BAND CENTER

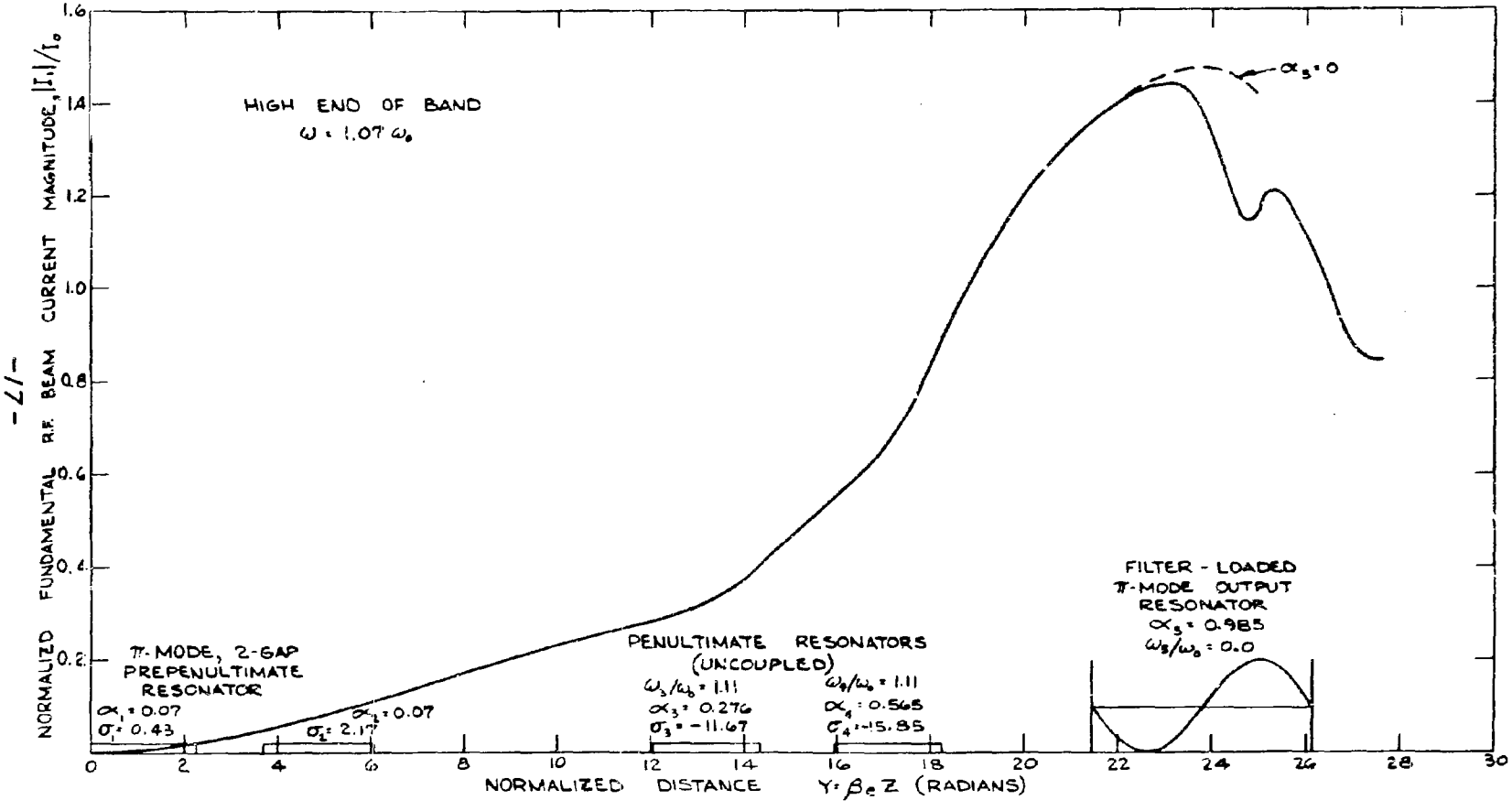

FIG. 7 FUNDAMENTAL RF BEAM CURRENT VS. DISTANCE IN THE KLYSTRON OUTPUT REGION AT THE UPPER BAND EDGE.

III. SMALL-SIGNAL ANALYSIS OF THE BUNCHER SECTION

A. Introduction

In the previous section it was shown that an output power variation of less than 1 db can be obtained over a 14 percent range of frequencies with the particular output resonator assumed, provided the rf current driving that resonator is approximately constant across the band. The large-signal analysis, in which that rf drive current was nearly constant, was started at the fourth (prepenultimate) resonator of the tube rather than at the input. It is natural to question whether or not, starting from the input resonator, a reasonable buncher section can be designed which will provide the desired rf current to the output resonator. The small-signal computer program was used to answer this question. (It would have been costly and time consuming to have carried out the large-signal analysis from the input of the tube at all five frequencies investigated. This is because of the nature of the large-signal computer program, in which the klystron is analyzed one resonator at a time in a sequential manner.)

It will be seen in this section that it is possible to design a buncher with a small-signal gain variation of less than 1 db over a 14 percent bandwidth, with a gain level of about 36 db, and with reasonable power dissipation in the loads of the externally-loaded resonators. In addition, the small-signal rf voltages and currents of this buncher are compared with the large-signal voltages and currents from the previous section.

B. Small-Signal Gain-Bandwidth Responses

Some small-signal gain and phase vs. frequency responses of the klystron buncher section have been presented in earlier reports of this contract. These responses were not presented as finalized, but only to illustrate the feasibility of obtaining a reasonably flat gain over a 14 percent bandwidth, and at a reasonable gain level. Final refinement of the buncher section was postponed until the results of the large-signal analysis could be used to more closely define the desired buncher characteristics. Once these results were known (that the rf drive current to the output resonator should be nearly constant across the band) the theoretical development of the buncher section was resumed.

1. Bunchers With Only Conventional Resonators

The klystron model used for the latest calculations on buncher sections containing only conventional single-gap resonators is shown in Fig. 8. This is the same model that was used in the earlier calculations with the following exceptions (See pages 70 and 74 of the First Quarterly Report): the tube length was increased slightly to eliminate a gain zero near the high end of the band, the R/Q values used were based on cold test information, and the output resonator was changed to a π-mode resonator to be consistent with the large-signal analysis. In addition, the assumed normalized length of each interaction gap was changed from 1.0 to 1.2 radians. Otherwise all the tube parameters were the same as listed in

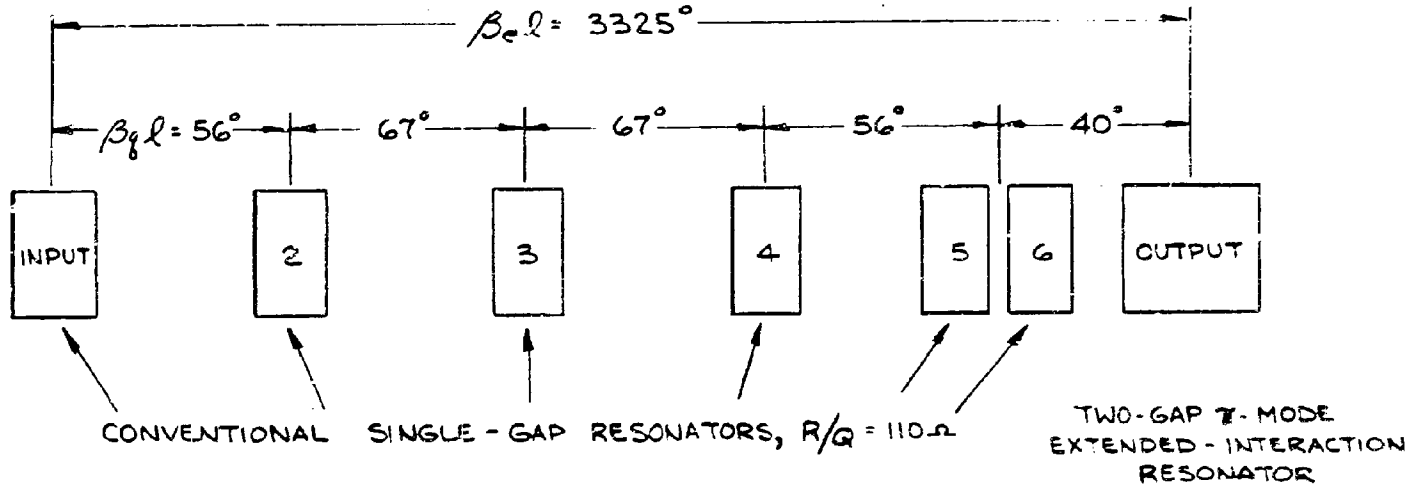

Fig. 8 - Final conventional-buncher-cavity klystron model.

Section I of the First Quarterly Report.

As before, in order to eliminate the small-signal response of the output resonator from the calculations and thus obtain a true picture of the response of the buncher section only, the Q of the output resonator was set equal to unity. The overall impedance of the resonator was, however, maintained equal to the correct value (which for the latest calculations was the impedance of the filter-loaded resonator assumed in the large-signal analysis).

The gain vs. frequency response of one conventional-resonator buncher section whose small-signal gain is flat within 1 db over the 14 percent band is shown in Fig. 9. The tuning and total Q of each resonator is indicated along the bottom of the figure. The first four resonators are assumed to be externally loaded while the penultimate resonators are loaded only by the beam ($Q_B = 134$ for all the buncher resonators). Calculations showing the power dissipation in the resonator loads to be reasonable are included later in this section. The phase vs. frequency response of this buncher, not including the linear variation due to the beam transit time, is shown in Fig. 10.

The results displayed in these two figures illustrate the feasibility of producing a klystron which has a saturated gain of over 30 db across a 14 percent band, and which contains only conventional resonators. In part C of this section the

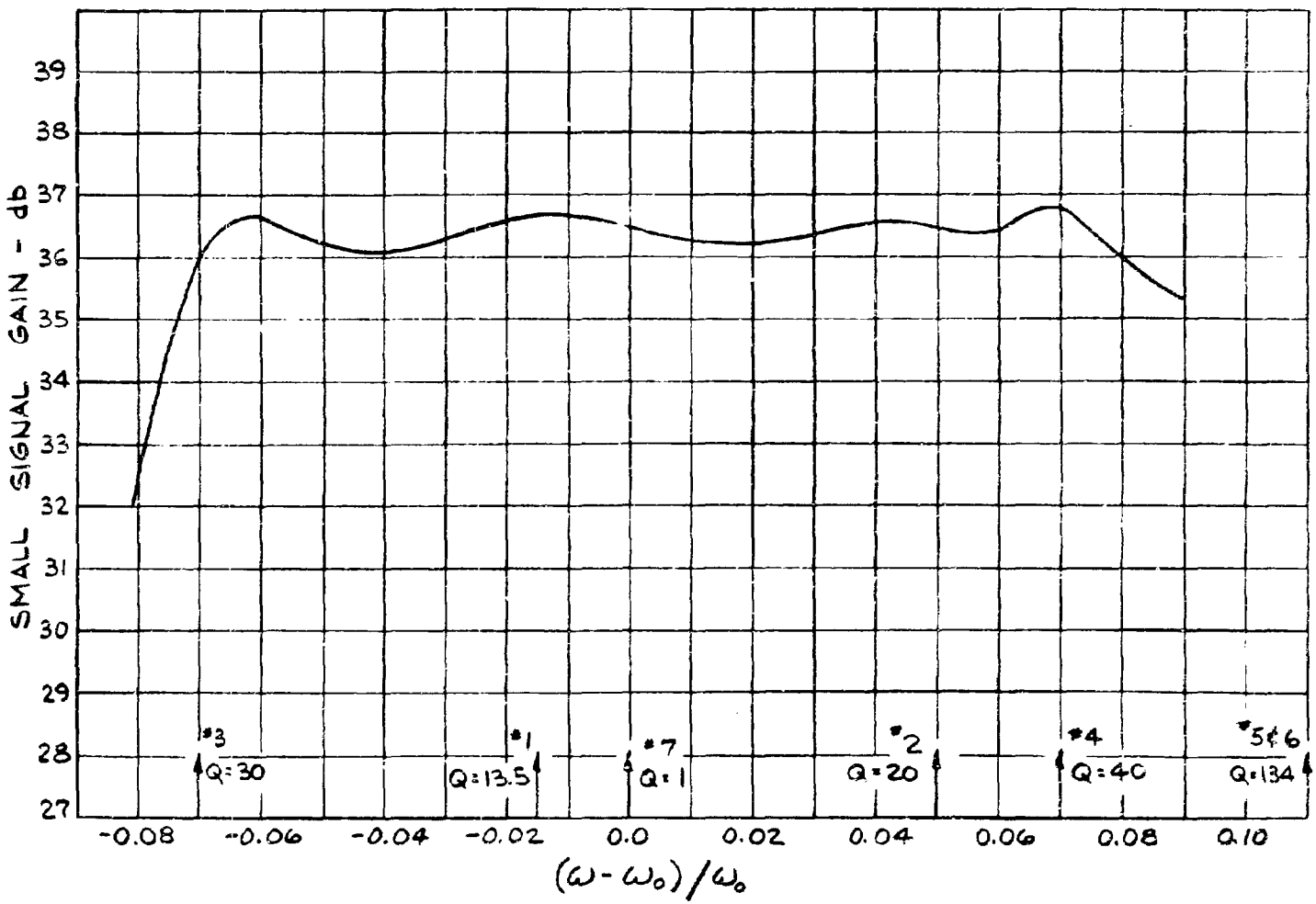

Fig. 9 - Computed gain vs. frequency characteristics of the klystron model shown in Fig. 8.

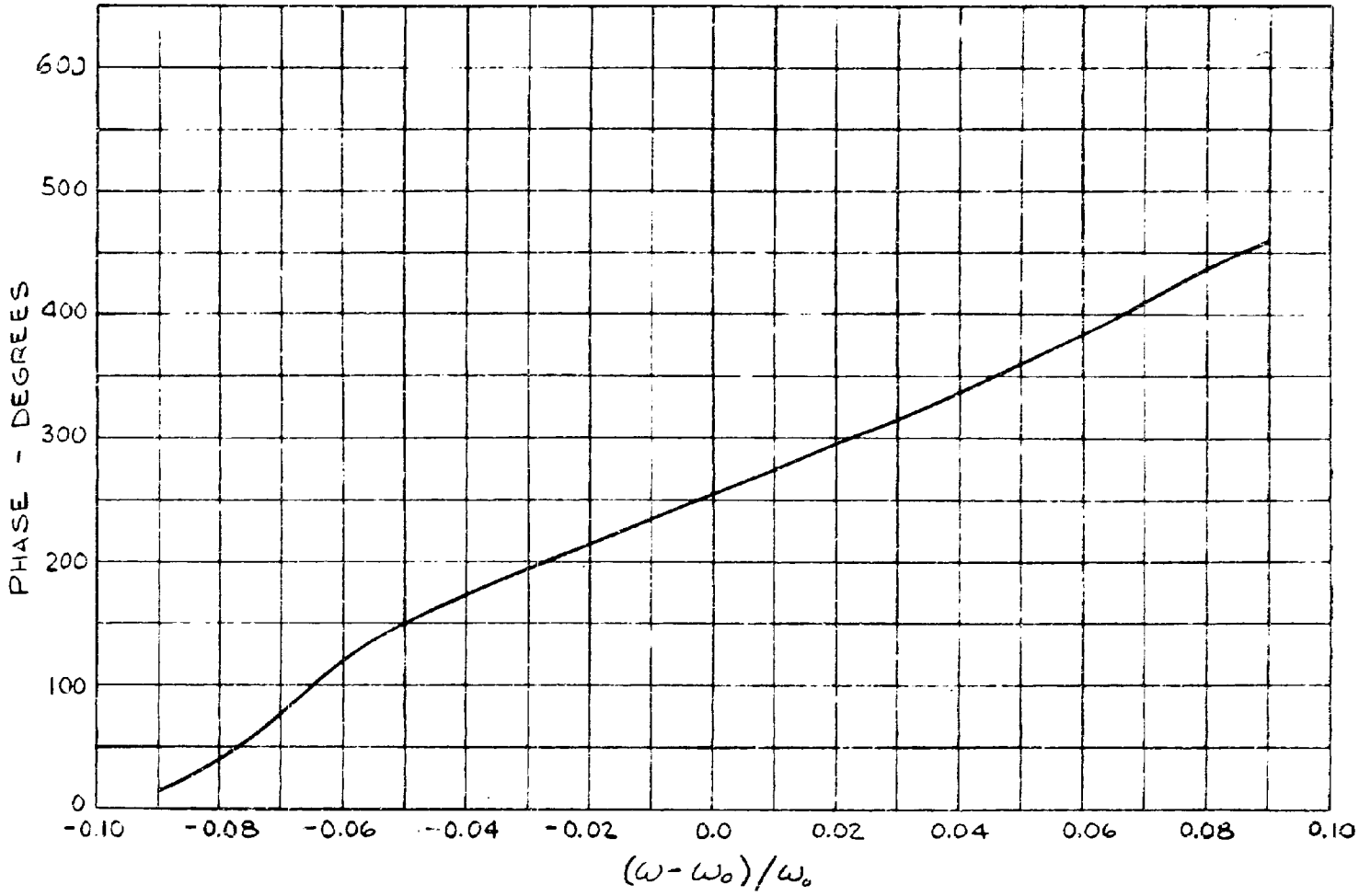

Fig. 10 - Computed phase vs. frequency curve of the klystron model described by Figs. 8 and 9.

characteristics of the particular buncher presented above will be related to the characteristics assumed in the large-signal analysis.

2. Bunchers With Extended-Interaction Resonators

Small-signal gain and phase vs. frequency calculations were also performed on buncher sections in which the first four resonators of Fig. 8 were replaced by two-gap π-mode extended-interaction resonators. The earliest gain-bandwidth calculations, presented in the First Quarterly Report, suggested that this type of buncher is superior to conventional-resonator bunchers. But these preliminary calculations were done before the computer program had been modified to account for the frequency variation of the parameters (e.g., coupling coefficients and beam-loading conductance). In addition, the assumed values of R/Q were considerably higher than have been obtained in cold test.

In the latest gain-bandwidth calculations, it has not been possible to obtain as good a performance from extended-interaction-resonator bunchers as from conventional-cavity bunchers. A typical gain vs. frequency curve obtained is plotted in Fig. 11. The model used for this calculation is shown in Fig. 12. The R/Q values used for the second, third, and fourth resonators are based on cold-test measurements (See the Second and Third Quarterly Reports). The R/Q value of the input resonator, lower because of its greater length, was

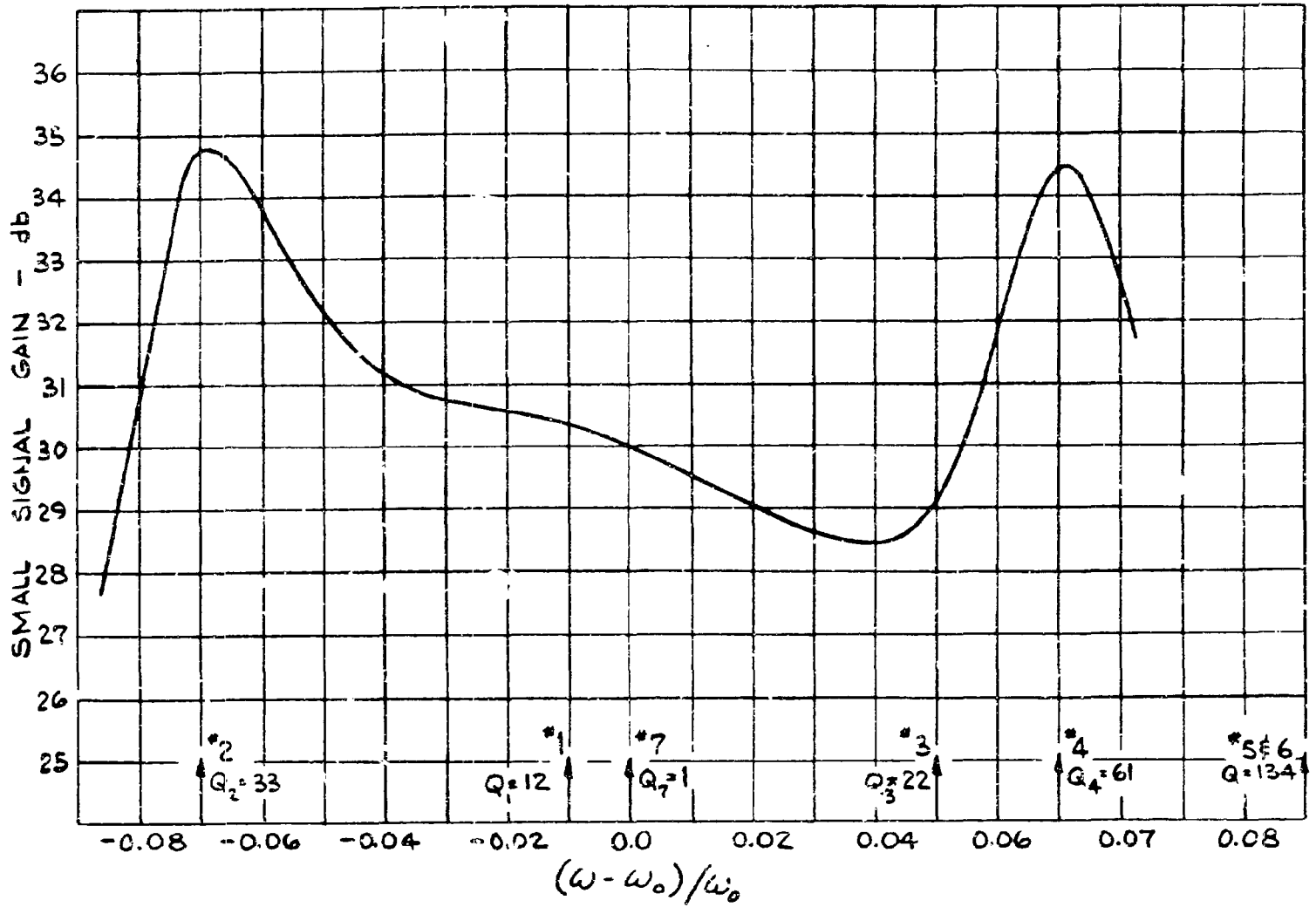

Fig. 11 - Computed gain vs. frequency response of the klystron model shown in Fig. 12.

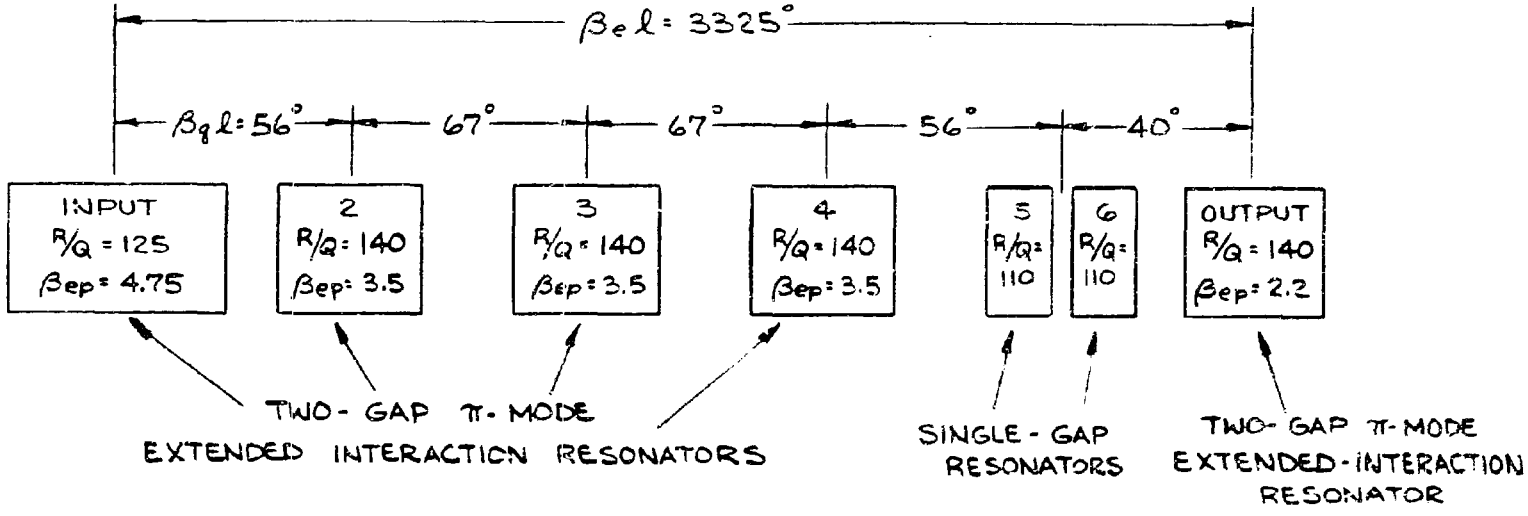

Fig. 12 - Extended-interaction klystron model.

estimated. The last three resonators of the model are the same as in Fig. 8.

It is apparent that the gain curve of Fig. 11 is not as desirable as the gain curve of Fig. 9 and, by comparison, is not acceptable. Various other combinations of resonator spacings, tunings, and Q's were tried with extended-interaction bunchers, but in no case tried could a flat gain response be obtained. Furthermore, in no case tried was the gain level appreciably higher than in Fig. 9.

It is believed that the explanation for the poorer performance of these bunchers lies mainly in the rapid frequency variation of the coupling coefficients and beam loading of the extended-interaction resonators combined with the fact that their R/Q values are only a little greater than those of the conventional resonators. The relatively low values of R/Q are a result of a number of factors. For one, in this contract we have restricted ourselves to single-mode extended-interaction resonators. In order to assure single-mode operation, the resonator cold bandwidth must be large, with a consequent sacrifice in the R/Q. Another factor in the low R/Q is the rather large drift tube diameter to resonator diameter ratio. This ratio in turn was determined by the chosen power level, frequency, and the reasonable values assumed for the beam perveance, beam area convergence ratio, and beam diameter to drift tube diameter ratio.

In view of our findings to date, we conclude that conventional resonators are to be preferred in the buncher section at this power level and frequency. It should be pointed out that this conclusion does not necessarily hold at lower power levels and/or lower frequencies. Nor would it necessarily hold if mode overlapping were allowed and made use of in the extended-interaction resonators.

C. Comparisons Between the Small-Signal and Large-Signal Analyses

The results of the large-signal analysis, presented in Section II, showed that if a filter-loaded output resonator is to be used, the rf drive current to that resonator should be approximately constant across the band. Starting at the fourth (prepenultimate) resonator of the tube model (Fig. 8), the large-signal analysis also demonstrated the possibility of obtaining a constant saturation-level rf current at the output resonator at each frequency. The small-signal computer program was used to study the buncher section from the input. In part B of this section a buncher response was presented showing nearly constant small-signal gain across the band. Since constant buncher gain, combined with constant input power, implies constant drive current to the output resonator, both the large-signal and small-signal calculations of the overall buncher response are in close agreement. However, because the large-signal computations were begun at the fourth resonator of the tube, instead of at the input, a more detailed comparison was made between the results of the two analyses.

(The reason for starting the large-signal analysis at the fourth resonator of the tube lies in the nature of the large-signal computer program. The program does not compute the impedance of each resonator from input values of Q, R/Q, and resonator tuning. Rather, the basic input quantities to the program are the beam parameters and the location, field form, and rf voltage (magnitude and phase angle) of each interaction gap. The program then calculates the rf beam current as a function of distance and, at each gap, the induced rf current, impedance, and conversion efficiency. If the calculated impedance at any gap is incorrect, the assumed value of gap voltage magnitude and/or phase angle must be adjusted to correct the impedance. The proper voltage for any one gap can usually be estimated very closely provided the rf beam current arriving from the preceding gaps is known. For this reason, the tube is usually analyzed one resonator at a time, in sequence. It is therefore te costly and time consuming to analyze a complete seven-cavity tube with this computer program, especially at many different frequencies. A new large-signal computer program which will automatically iterate the gap impedances is under development, but is not yet complete. The large-signal analysis was therefore begun at the cavity immediately preceding the two penultimate resonators.)

The comparison between the two analyses was carried out by looking at the rf currents and gap voltages from the two computer programs. The large-signal currents and voltages from Section II

were compared with the small-signal currents and voltages from the buncher section of Fig. 9. It would not be expected that the magnitudes of these voltages and currents from the two programs would be the same, but it is reasonable to assume that the manner in which they vary with frequency should be similar.

The large-signal rf gap voltages and the rf current driving the output resonator were listed in Table I, page 6. The small-signal gap voltages for the buncher of Fig. 9 are plotted as a function of frequency in Fig. 13. The small-signal rf currents at the entrance to each resonator are shown in Fig. 14. (The input current to the first resonator was equal to unity at all frequencies.)

An examination of Fig. 14 shows that the current at the output resonator from the small-signal program is constant within a few percent over the band, as it was in the large-signal case. The two currents are compared more directly in Fig. 15 where they are plotted normalized, separately in each program, to the value at the center of the band. The choice of the normalization frequency was arbitrary. In both cases, the current varies less than five percent from the value at the center of the band.

One important difference between the small-signal and large-signal currents was revealed by the comparison between the two analyses. For the purpose of the large-signal calculations, the rf current at the fourth resonator was assumed to be zero. An inspection of the current at the fourth resonator in the small-signal

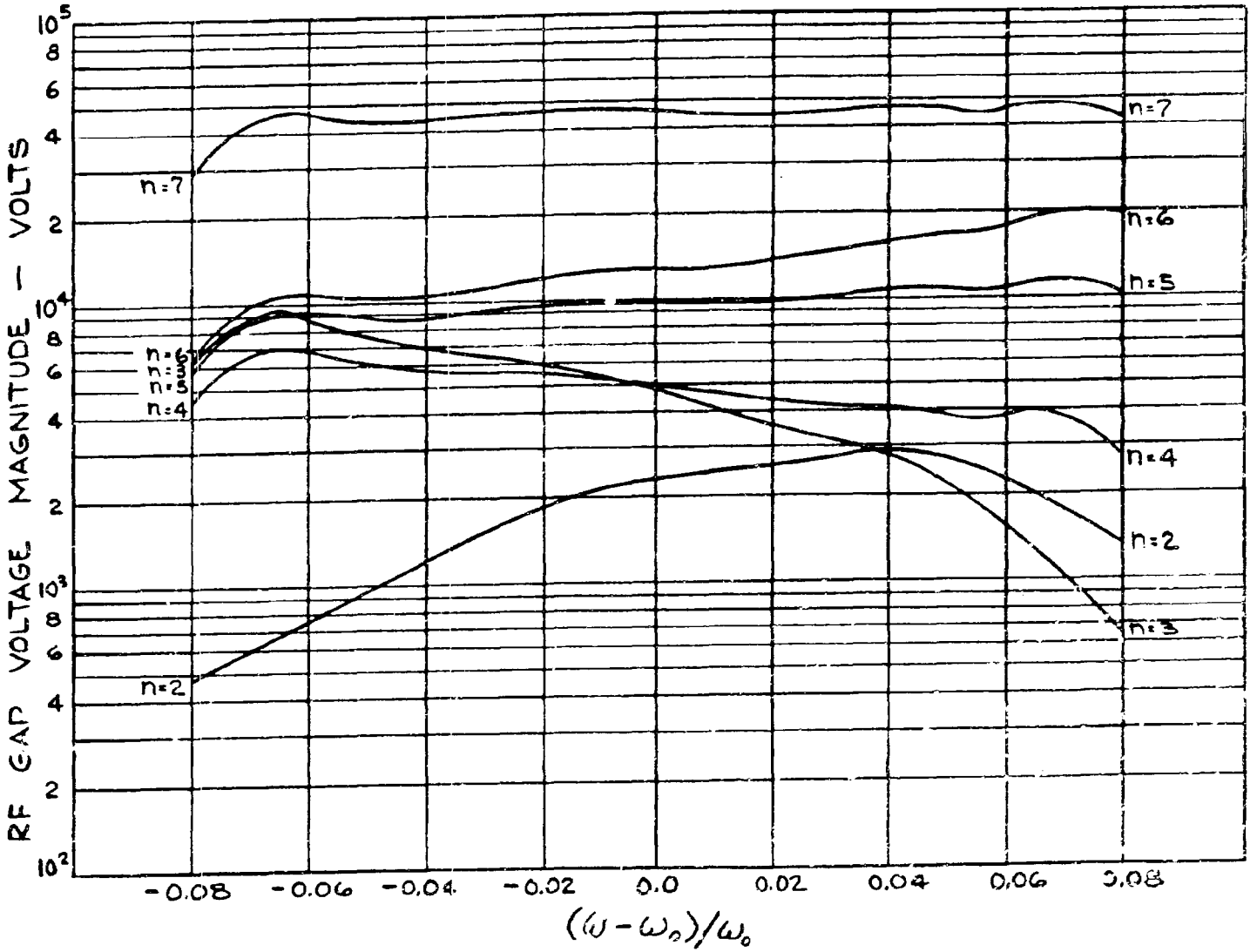

Fig. 13 - RF gap voltages of the klystron model described by Figs. 8 and 9 as computed by the small-signal program.

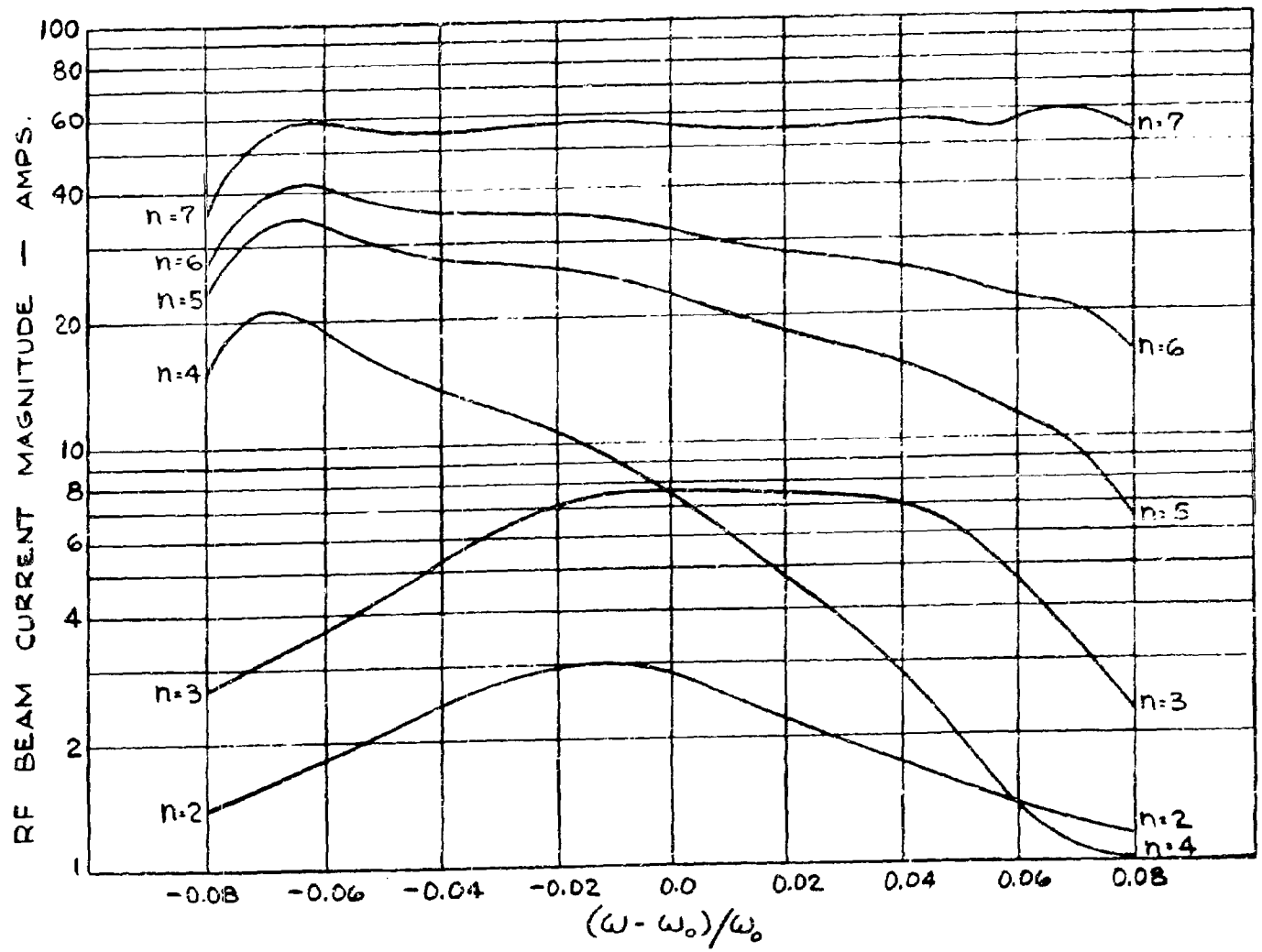

Fig. 14 - RF beam current at each gap of the klystron model described by Figs. 8 and 9 as computed by the small-signal program.

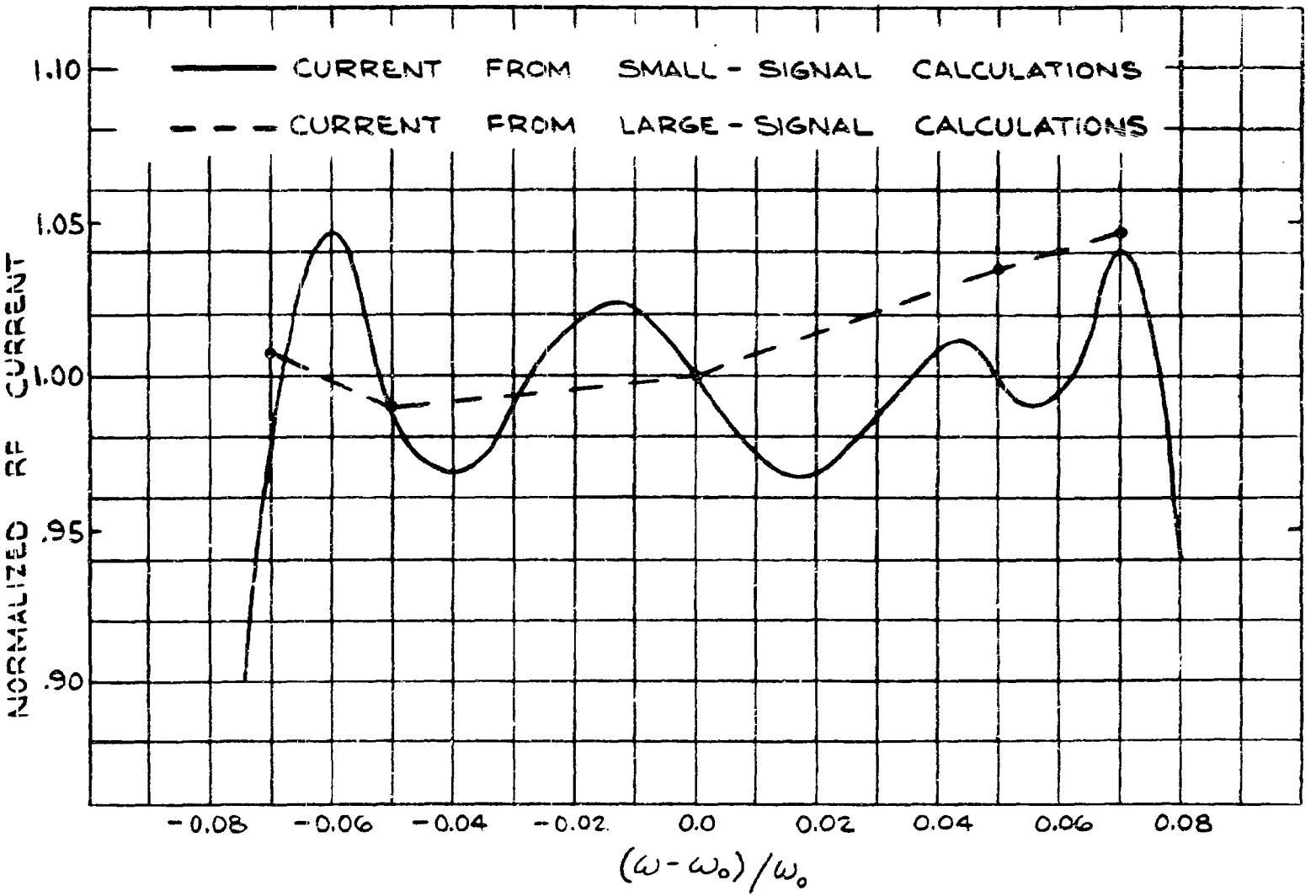

Fig. 15 - RF beam current at the output resonator.

calculations (Fig. 14) indicates that this assumption was reasonable at the high end of the band but is questionable at the low end of the band.

To evaluate the error introduced into the original output efficiency calculations by this assumption, the large-signal computations were repeated at the low end of the band starting from the third resonator. The entire analysis was performed in just two computer runs, rather than one resonator at a time as is usually done. All four buncher resonators were analyzed in the first computer run by choosing the two penultimate voltages to be the same as before, and setting the voltages on the third and fourth resonators to be in the same ratio to the first penultimate voltage as they were in the small-signal case under comparison. The output resonator was added in the second computer run, which started from data stored in the first run. Also, to be consistent with the small-signal case, the fourth resonator was assumed to be a single-gap resonator instead of the two-gap extended-interaction resonator used previously. The results of this new analysis are displayed in Fig. 16 (See Fig. 5, page 15 for comparison). As can be seen, the rf beam current driving the output resonator is lower than before, and the peak of the current from the buncher is located beyond the center of the resonator gap rather than slightly in front of it as in the previous case. Furthermore, the resulting impedance values for the two penultimate resonators are slightly high (indicated on the figure by the lower values of detuning). To correct the

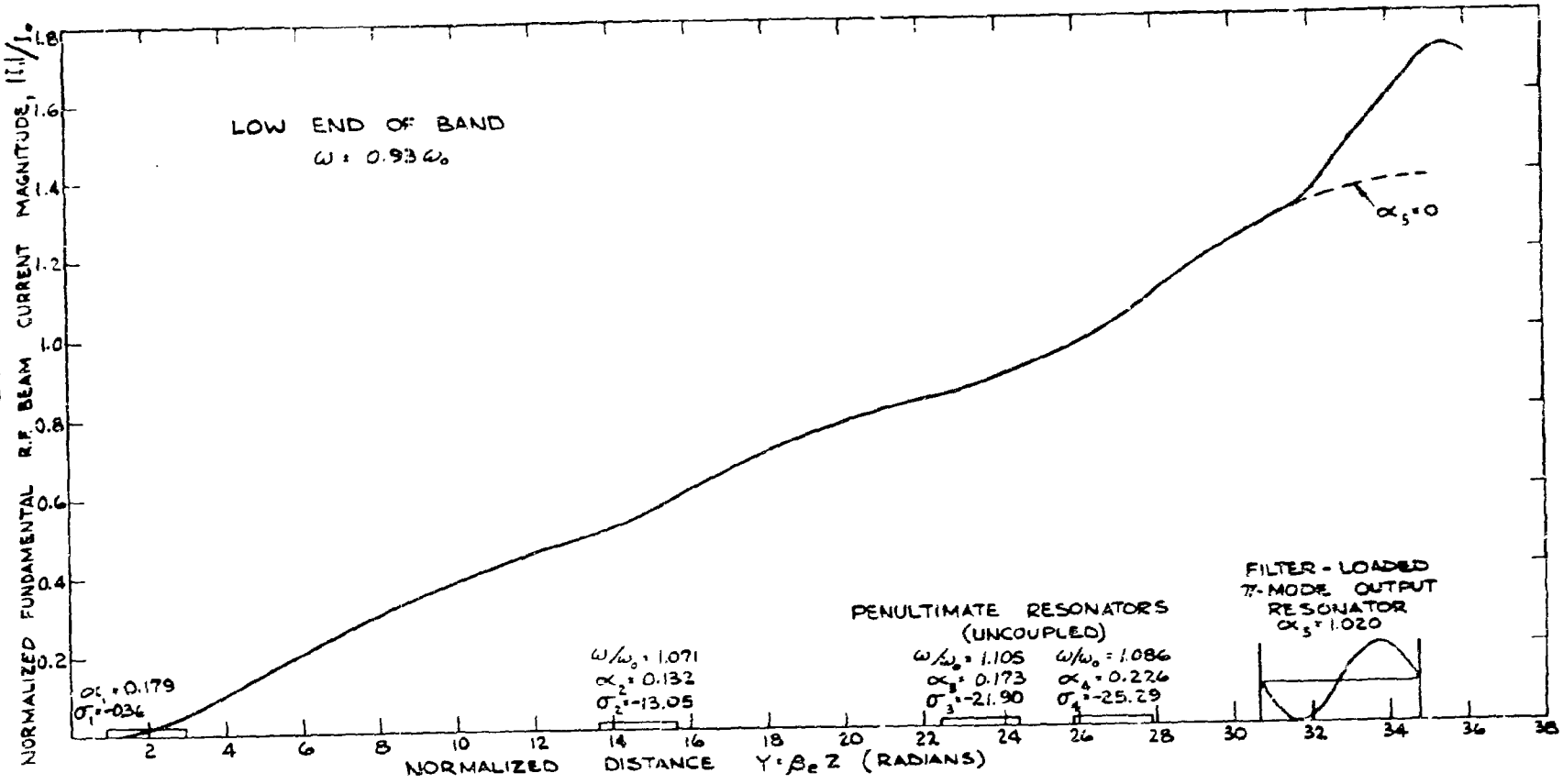

F.G. 16 FUNDAMENTAL RF BEAM CURRENT VS DISTANCE IN THE KLYSTRON OUTPUT REGION AT THE LOWER BAND EDGE

impedances, the penultimate gap voltages should be lowered which in turn would further lower the rf beam current beyond the penultimate system. However, because the beam is not completely bunched at the output resonator gap, there is a greater remodulation of the beam within the resonator than before. The output conversion efficiency in this new case is 49.8 percent, which is higher than the former value of 47.5 percent at this frequency. Had the penultimate impedance values been corrected, the new value of efficiency would have been lower and probably closer to the previous value.

From the outcome of this last analysis, it is apparent that only a small error was introduced at the low end of the band by starting the large-signal calculations at the fourth resonator, rather than at the third or an earlier resonator. In addition, since the assumption of zero rf current at the fourth resonator is most seriously violated at the lower band edge, it is reasonable to assume that the efficiency values computed at the other frequencies would not have been significantly different had the large-signal analysis been started at an earlier resonator. We feel therefore that the efficiency-bandwidth conclusions reached in Section II are valid.

D. Power Dissipation in the Buncher Loads

The first four buncher resonators would have to be externally loaded to achieve the Q values assumed in the small-signal analysis. The power dissipated in the loads of these resonators can be calculated from

$$P_L = \frac{1}{2} \frac{|V|^2}{(R/Q) Q_e} \qquad (3)$$

Where

V = rf gap voltage

R/Q = resonator impedance quality factor

Q_e = external Q

The highest power dissipation will be in the loads of the third and fourth resonators where the gap voltages are the highest. The curves of Fig. 13 show that the gap voltages on these resonators are a maximum at the lower band edge. This is the frequency at which the power calculations were performed. The actual gap voltages used in the calculations were obtained from the large-signal analysis (See Fig. 16). The pertinent quantities are listed in Table III below.

TABLE III

Resonator Number	Q_L	Q_B	Q_E	R/Q	$\alpha = \frac{\|V\|}{V_o}$
3	30	134	39	110	.18
4	40	134	57	110	.13

If these numbers are substituted into Eq. (3), the average power dissipated in the loads during the time the beam is on is obtained. For the third resonator, this power turns out to be 74 kW,

and for the fourth resonator, 26 kW. If the tube were operated at a pulse duty factor of 0.01, the average power dissipated in the loads of these resonators would be 740 watts and 260 watts, respectively.

The beam voltage and beam current assumed in both the large-signal and small-signal analyses were 140 kV and 105 A. The corresponding peak beam power is 14.7 MW. At an efficiency of 48 percent, the peak rf output power would be approximately 7 MW and, at the duty factor of 0.01, the average rf power would be 70 kW. The maximum power dissipated in any one buncher load would be less than one kilowatt, which is not unreasonably high for a tube of this power level. The maximum total power dissipated in the buncher loads would be about 1.5 percent of the rf output power. In view of these results, we believe that the conventional-resonator buncher described in this report is a practical one.

IV. STABILITY OF TWO-GAP FILTER-LOADED RESONATORS

A. Introduction

In order to theoretically investigate the stability of the two-gap filter-loaded output resonators studied in this program, it was necessary to develop a new method for calculating the stability of extended-interaction resonators. The theoretical basis for the method is presented in this section in terms valid for extended-interaction resonators having any number of interaction gaps and any number of sections in the filter load. The application of this method to a two-gap π-mode output resonator with a single-section filter is described. The degree of stability of the resonator in each of its main modes was calculated at a number of beam voltages from 50 kV to 140 kV. The results show that the resonator is stable over the range of voltages investigated.

B. Stability Criterion

The conventional criterion used for determining the stability of a resonator is expressed by

$$G_e + G_c > 0 \quad , \tag{4}$$

where G_e is the small-signal beam loading conductance and G_c is the total equivalent circuit conductance of the resonator. The calculation of G_e can be readily performed by using Eq. (43) in the First Quarterly Report provided the gap voltage distribution and the oscillation frequency are known. This is normally the case for high-Q

single-mode resonators. For a heavily loaded resonator with a filter output, neither the gap voltage distribution or the likely oscillation frequencies are known. We shall, therefore, use a more general approach in the following analysis which does not require a previous knowledge of the oscillation frequency and the gap voltage distribution in the resonator.

The analysis is based upon Eq. (57) in the First Quarterly Report.

$$\left[\underset{\sim}{Y}_e + \underset{\sim}{Y}_c\right] \underset{\sim}{V} = -I_{max} \underset{\sim}{g} + \frac{U_{min}}{W} \underset{\sim}{\Delta} \qquad (5)$$

Equation (5) gives the gap voltages, expressed by the gap voltage vector $\underset{\sim}{V}$, for a given rf modulation of the beam entering the resonator. $\underset{\sim}{Y}_e$ and $\underset{\sim}{Y}_c$ are the electronic and circuit interaction matrices. The rf modulation on the beam is characterized by an rf current I and a kinetic voltage U. For convenience the rf beam parameters are expressed in terms of the current and the kinetic voltage at the position where the current is maximum. It should be noted that the maximum value of the rf beam current I_{max} always occurs at the same position as the minimum value of the kinetic voltage U_{min}. As will be apparent in the next paragraph, the definitions of the matrices $\underset{\sim}{g}$ and $\underset{\sim}{\Delta}$ are not important in the following discussion. The reader is therefore referred to the First Quarterly Report for the definition of these matrices.

In the stability calculations, we are interested in the response of the resonator to the dc beam. In this case, the rf current modulation I_{max} and the kinetic voltage U_{min} of the primary beam are

equal to zero. By introducing $I_{max} = U_{min} = 0$ into Eq. (5) we get

$$\left[\underset{\sim}{Y}_e + \underset{\sim}{Y}_c\right] \underset{\sim}{V} = 0 \quad . \tag{6}$$

The derivation of Eq. (5) was based upon a linear small-signal theory. Saturation effects are not described by the equation. Therefore, once the resonator has been excited, the conditions of stability or instability are characterized by an exponential decrease or increase in the amplitude of the gap voltage vector $\underset{\sim}{V}$ with time. This behavior is described mathematically by using the concept of complex frequency

$$\omega = \omega' + j\sigma \tag{7}$$

where both ω' and σ are real. The resonator system is stable when $\sigma > 0$ and is unstable when $\sigma < 0$.

The complex frequency is a standard concept used in circuit analysis. The required modification of the circuit matrix is obtained simply by substituting the complex frequency for the real frequency. The direct substitution of frequencies is not directly valid in the electronic admittance matrix. The use of the complex frequency in the electronic interaction equations affects the space-charge reduction factor and the gap coupling coefficient. The standard derivation of these two parameters is based upon a real frequency (steady state condition). In order to use the standard space-charge reduction factor and the beam coupling coefficient, we shall restrict the

analyses to cases where the voltage amplitude is slowly varying with time ($\sigma << \omega$). This is not a severe restriction since we are primarily interested in the sign of σ.

Equation (6) represents a set of linear homogenous equations in the gap voltages V_p. In order that $\underset{\sim}{V}$ be non-zero, the admittance determinant must vanish.

$$\left| \underset{\sim}{Y}_e + \underset{\sim}{Y}_c \right| = 0 \qquad (8)$$

Equation (8) gives the characteristic complex frequencies of the resonator with the beam present and is the basic equation for the stability calculation.

C. Circuit Matrix

The equivalent circuit used to represent the π-mode single-section filter-loaded resonator is shown in Fig. 17.

Referring to the figure it is assumed that the beam interacts with the two first cavities, while the third cavity represents the loaded filter. The three resonator cells are coupled inductively by the coupling inductances L_{01} and L_{02}. The circuit admittance matrix in Eq. (8) is defined by the relation

$$\underset{\sim}{I} = \underset{\sim}{Y}_c \underset{\sim}{V} \qquad (9)$$

where $\underset{\sim}{I}$ and $\underset{\sim}{V}$ are the induced current and gap voltage vectors represented by the column vectors

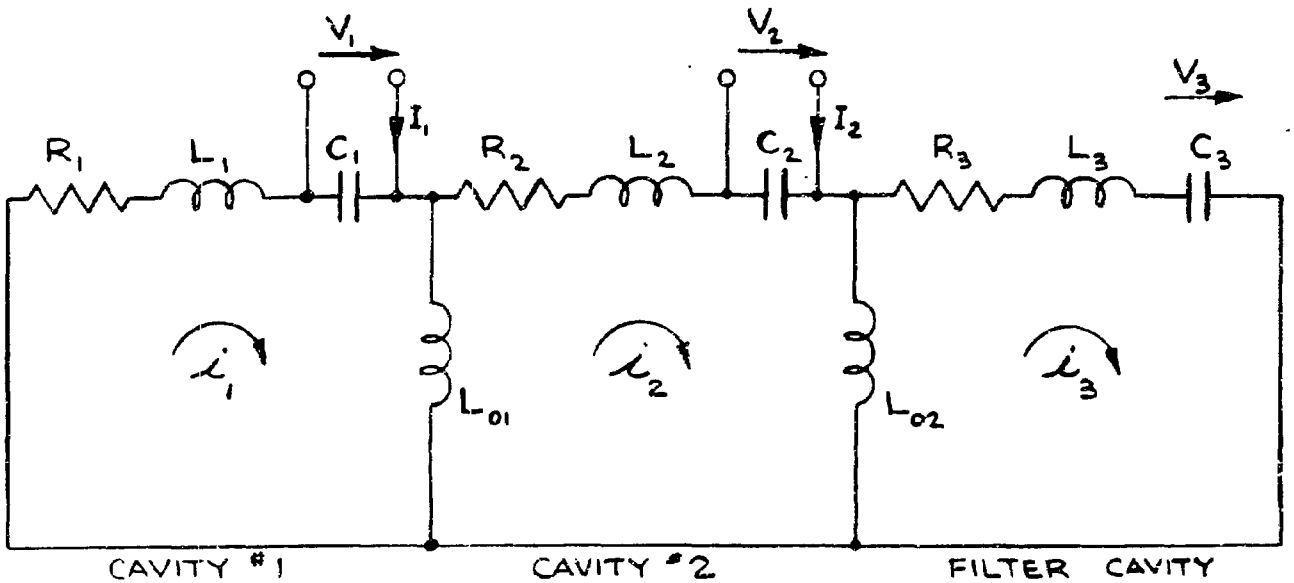

Fig. 17 - Equivalent circuit representing a two-gap resonator with a single-section filter load.

$$\underset{\sim}{I} = \begin{bmatrix} I_1 \\ I_2 \\ 0 \end{bmatrix} \quad \text{and} \quad \underset{\sim}{V} = \begin{bmatrix} V_1 \\ V_2 \\ V_3 \end{bmatrix} \tag{10}$$

The elements in the circuit admittance matrix are found by applying Kirchhoff's laws to each mesh in the equivalent circuit.

In the detailed derivation of the circuit admittance matrix we assumed that the reactive components in the two first cells are identical: $L_1 = L_2$ and $C_1 = C_2$. The expression used in the calculations of the gap voltages was

$$V_p = C_p (I_p - i_p) \approx -C_p i_p \tag{11}$$

which implies that the induced currents are neglected compared with the loop currents.

D. Electronic Admittance Matrix

The beam interacts with only two of the three cells in the equivalent circuit of Fig. 17.

$$\underset{\sim}{Y}_e = \begin{bmatrix} Y_{e,1} & 0 & 0 \\ Y_{2,1} & Y_{e,2} & 0 \\ 0 & 0 & 0 \end{bmatrix} \tag{12}$$

where $Y_{e,p}$ is the electronic beam loading admittance for the p-th interaction gap and $Y_{2,1}$ is the transfer admittance between the first and second gaps. We are assuming that the two interaction gaps have

identical geometry; therefore

$$Y_{e,1} = Y_{e,2} = Y_e \quad . \tag{13}$$

The beam loading admittance Y_e is in general complex. However, the susceptive part of the admittance results only in a negligible detuning of the resonator and is neglected in the stability calculations. We shall therefore replace the beam loading admittance by the beam loading conductance G_e. Therefore,

$$\underset{\sim}{Y}_e = \begin{bmatrix} G_e & 0 & 0 \\ Y_{2,1} & G_e & 0 \\ 0 & 0 & 0 \end{bmatrix} \tag{14}$$

The transfer admittance $Y_{2,1}$ and the beam loading conductance G_e can be derived from Eqs. (18) and (43) in the First Quarterly Report.

E. Selection of the Values of the Components in the Equivalent Circuit

In the calculations of the output efficiency described in the Third Quarterly Report, the filter-loaded two-gap extended-interaction output resonator was represented by the same two-mesh equivalent circuit used for a filter-loaded single-gap output resonator. This was a reasonable assumption since, as long as it is operating in a single mode, an extended-interaction resonator can be represented by the same equivalent circuit used to represent a single-gap cavity. The values of the components of the more complete equivalent circuit of Fig. 17 required for the stability calculations must be selected to yield the

same frequency variation of the interaction impedance as for the simplified circuit described above.

Since the beam-circuit interaction takes place only in the two first resonator gaps, the definition of the interaction impedance will be based upon the drive current and voltages in these two gaps alone. We shall assume that we have pure π-mode excitation currents and gap voltages.

A general combination of the gap voltages V_1, V_2, and V_3 and induced currents I_1 and I_2 can be expressed by the vector equations.

$$\underset{\sim}{V} = V_\pi \underset{\sim}{e}_\pi + V_{2\pi} \underset{\sim}{e}_{2\pi} + V_3 \underset{\sim}{e}_3 \tag{15}$$

$$\underset{\sim}{I} = I_\pi \underset{\sim}{e}_\pi + I_{2\pi} \underset{\sim}{e}_{2\pi} \tag{16}$$

where V_π, $V_{2\pi}$, I_π and $I_{2\pi}$ are the complex amplitudes of the π- and 2π-mode voltage and current modes. $\underset{\sim}{e}_\pi$ and $\underset{\sim}{e}_{2\pi}$ are the unit vectors for the π mode and the 2π mode defined by:

$$\underset{\sim}{e}_\pi = \frac{1}{\sqrt{2}} \begin{bmatrix} 1 \\ -1 \\ 0 \end{bmatrix} \tag{17}$$

and

$$\underset{\sim}{e}_{2\pi} = \frac{1}{\sqrt{2}} \begin{bmatrix} 1 \\ 1 \\ 0 \end{bmatrix} \tag{18}$$

$\underset{\sim}{e}_3$ is the unit vector for the gap voltage in the third resonator cell

$$\underset{\sim}{e}_3 = \begin{bmatrix} 0 \\ 0 \\ 1 \end{bmatrix} \tag{19}$$

We shall define the π mode interaction impedance Z_π by:

$$Z_\pi = \frac{V_\pi}{I_\pi} \tag{20}$$

The gap voltages can be expressed in terms of the induced current by Eq. (9)

$$\underset{\sim}{V} = \underset{\sim}{Y}_c^{-1} \underset{\sim}{I} = \underset{\sim}{Z}_c \underset{\sim}{I} \tag{21}$$

where $\underset{\sim}{Z}_c$ is the circuit impedance matrix.

The unit vectors are orthogonal and V_π can be found from

$$V_\pi = \tilde{e}_\pi \underset{\sim}{V} \tag{22}$$

where $\tilde{e}_\pi$ is the transpose of the unit vector $\underset{\sim}{e}_\pi$.

From Eqs. (20), (21), and (22) we obtain

$$Z_\pi = \frac{\tilde{e}_\pi \underset{\sim}{V}}{I_\pi} = \frac{\tilde{e}_\pi \underset{\sim}{Z}_c I_\pi \underset{\sim}{e}_\pi}{I_\pi} = \tilde{e}_\pi \underset{\sim}{Z}_c \underset{\sim}{e}_\pi \tag{23}$$

This impedance Z_π as predicted by the equivalent circuit of Fig. 17 was compared with the impedance Z_{11} predicted by the two-mesh circuit used in the efficiency calculations. In order to perform the comparison, it was necessary to relate the two different impedance

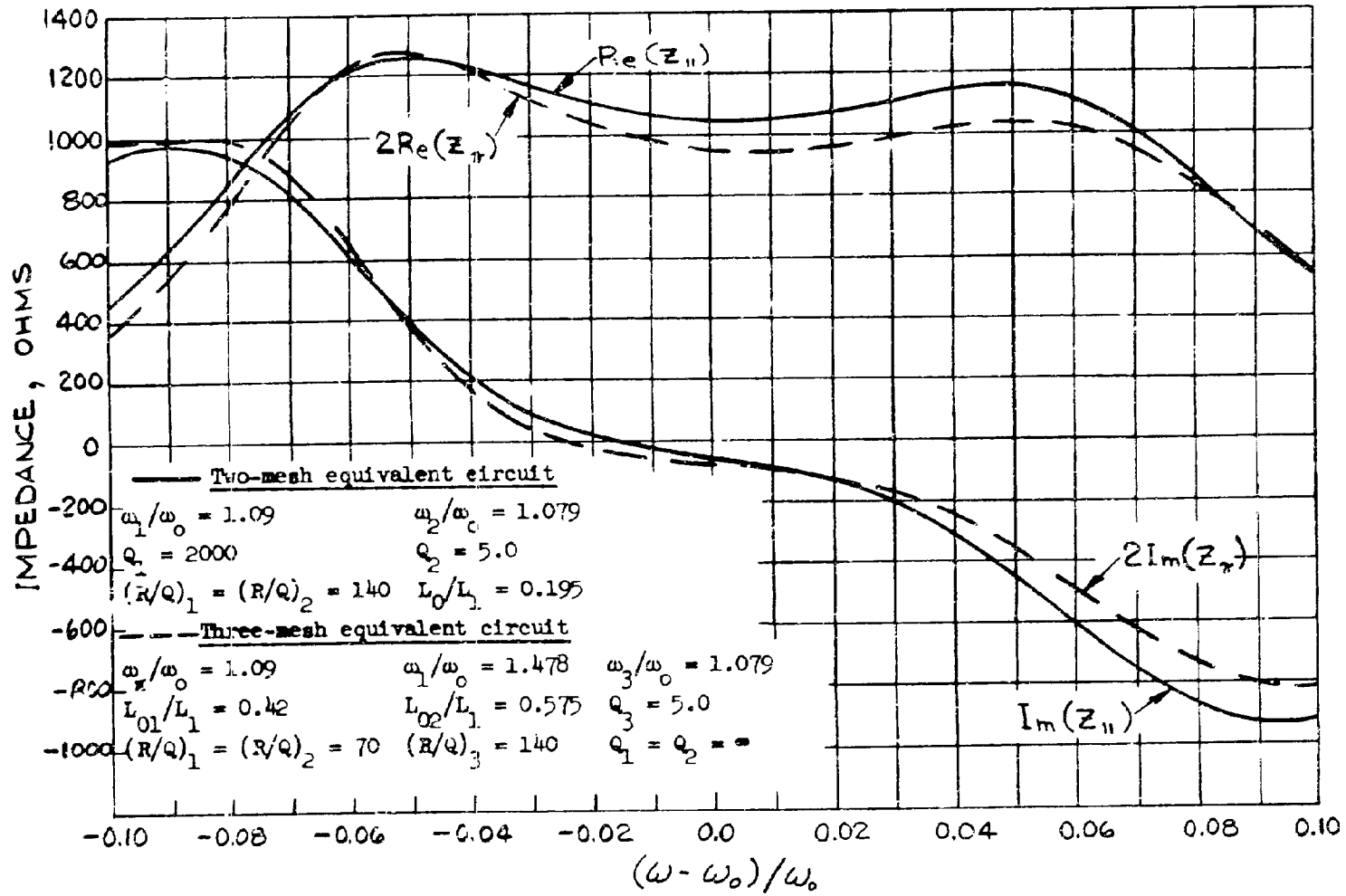

Fig. 18 - Filter-loaded output resonator interaction impedance as predicted by two different equivalent circuits.

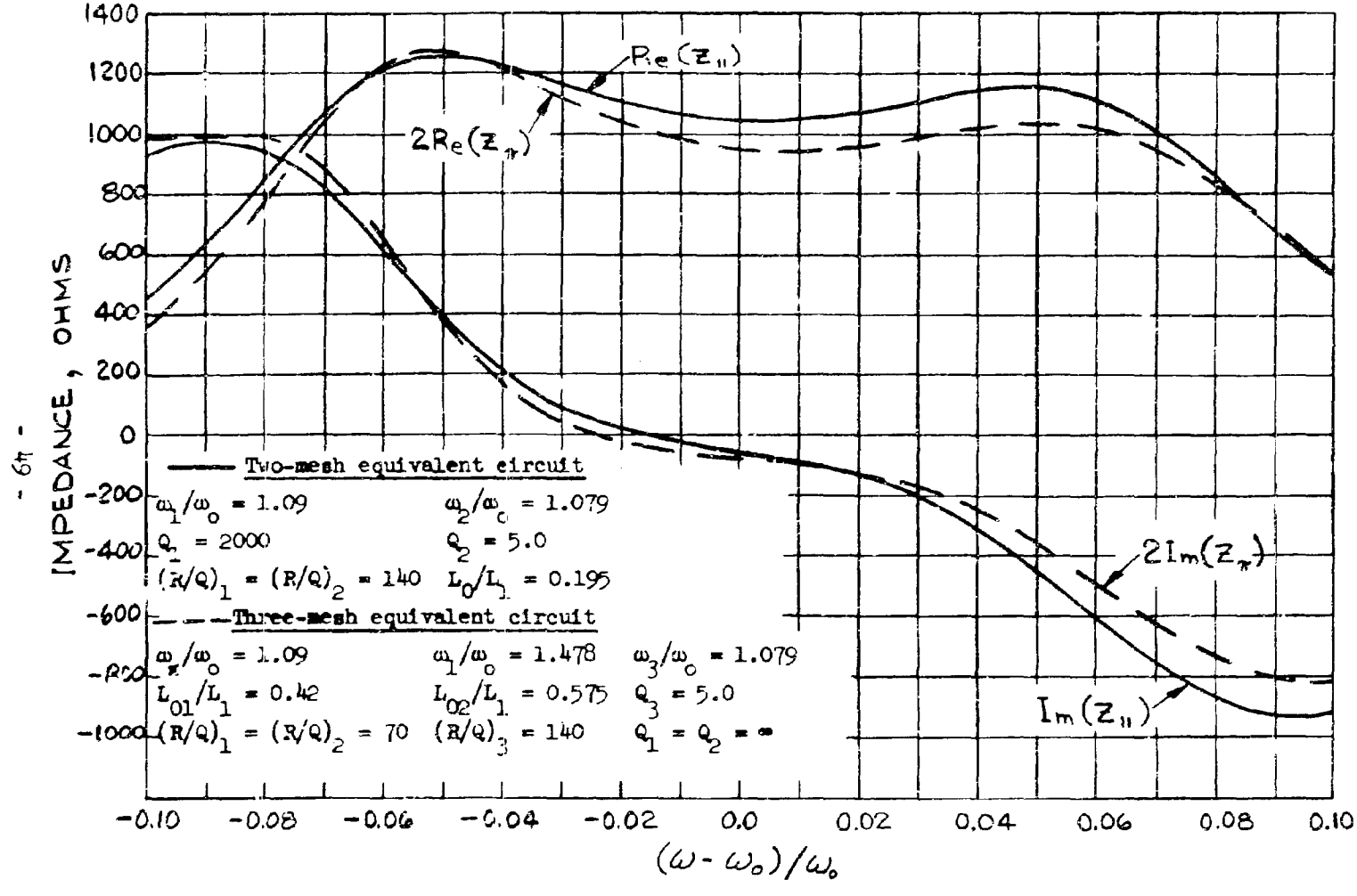

Fig. 18 - Filter-loaded output resonator interaction impedance as predicted by two different equivalent circuits.

SYMBOLS		DESCRIPTION
Two-Mesh Circuit	Three-Mesh Circuit	
ω_0	ω_0	Band-center frequency
ω_1	ω_π	Two-gap resonator π-mode frequency
ω_2	ω_3	Filter cavity frequency
--	ω_1	Uncoupled frequency of cavity #1
Q_1	--	π-mode Q of two-gap resonator
--	Q_1	Q of cavity #1
Q_2	Q_3	Filter cavity Q
$(R/Q)_1$	--	Overall R/Q of two-gap resonator in π mode
--	$(R/Q)_1$	R/Q of cavity #1 defined at π-mode frequency (= 1/2 π-mode R/Q of the two-gap resonator)
$(R/Q)_2$	$(R/Q)_3$	Filter cavity R/Q
L_0	L_{02}	Coupling inductance between filter cavity and two-gap resonator
--	L_{01}	Coupling inductance between cavity #1 and cavity #2
L_1	--	Equivalent inductance of two-gap resonator at π-mode frequency
--	L_1	Inductance of cavity #1

TABLE IV

Description of the notations used in Fig. 18.

used to determine the complex characteristic frequencies of the circuit is transcendental. This is due to the fact that the elements of the electronic matrix contain exponential and trigonometric functions of the frequency. The roots of the equation must therefore be found numerically. This was done by computing the value of the determinant as a function of the complex frequency on a digital computer. The complex frequency range where the roots would most likely be found was scanned using gradually smaller frequency steps until the roots were located with the desired accuracy.

The overall Q-factor of each mode can be found from its complex resonant frequency. The Q-factor is given by[1]

$$Q = \frac{\omega'}{2\sigma} \qquad (25)$$

This definition is based upon the rate of decay of the energy stored in the resonator. In cases where the resonant frequencies are close, the Q of a mode cannot be directly related to its response bandwidth.

As the beam loading in the resonator becomes more negative, the overall Q-factor will increase and eventually become negative at the point where the resonator breaks into oscillation.

From the knowledge of the overall Q-factors with and without the beam present we can judge how close the resonator is to breaking into oscillation. We shall define a stability parameter S by:

---

[1] D.F. Tuttle, "Network Synthesis," John Wiley and Sons, Inc., 1958, Vol. 1, p. 716.

$$S = \frac{\frac{1}{Q_c}}{\frac{1}{Q_{tot}} - \frac{1}{Q_c}} \qquad (26)$$

In Eq. (26), Q_c is the Q-factor of the resonator without the beam present and Q_{tot} is the Q-factor with the beam present.

Positive values of S indicate the presence of positive beam loading. Under these circumstances, the effective resonator circuit loading can be decreased to zero without initiating oscillation. Negative values of S indicate that negative beam loading is present. In this case the numerical value of S indicates the factor by which the Q-value of the circuit could be increased before oscillation begins. Values of S in the range $-1 < S < 0$ indicate that the resonator is unstable.

Computations were performed for beam voltages between 50 kV and 140 kV. The results are listed on Table V. The three characteristic modes of the resonator are identified by numbers between 1 and 3 according to decreasing values of the real part of the characteristic frequency. Mode 1 is close in frequency to the 2π mode, and mode 2 is close to the π mode, of the unloaded two-gap resonator. The real and imaginary parts ω' and σ of the characteristic frequencies are normalized to the center frequency ω_o of the operating band.

It is seen that all of the main resonator modes are stable over the calculated range of beam voltages. Mode 1 has the highest effective Q-factor. The negative beam loading of this mode is largest at a beam voltage of approximately 70 kV. The stability parameter S in this case is equal to -2.1. This provides sufficient safety against oscillation.

OPERATING VOLTAGE	MODE 1				MODE 2				MODE 3			
	$\frac{\omega'}{\omega_o}$	$\frac{\sigma}{\omega_o}$	Q	S	$\frac{\omega'}{\omega_o}$	$\frac{\sigma}{\omega_o}$	Q	S	$\frac{\omega'}{\omega_o}$	$\frac{\sigma}{\omega_o}$	Q	S
No beam	1.372	.00699	98	∞	1.070	.0532	10.0	∞	.935	.0374	12.5	∞
140 kV	1.380	.00855	81	4.6	1.065	.0536	9.9	82	.935	.0343	13.6	-12
100 kV	1.378	.00550	125	-4.6	1.065	.0555	9.6	21	.934	.0340	13.7	-11
70 kV	1.375	.00367	187	-2.1	1.066	.0576	9.3	12	.932	.0355	13.1	-21
50 kV	1.370	.00438	156	-2.7	1.068	.0589	9.1	9	.931	.0371	12.6	-230

TABLE V

Normalized complex characteristic frequencies, Q-factors, and values of the stability parameter S for the three characteristic modes of the two-gap single-section filter-loaded output resonator at various beam voltages.

V. TWO-GAP FILTER-LOADED RESONATOR COLD TEST

A. Introduction

Cold testing of a two-gap π-mode extended-interaction output resonator with single-section filter loading has been carried out in parallel with the theoretical investigation of the characteristics of this type of resonator (See Sections II and IV). The results have been encouraging, showing the possibility of obtaining a resonator impedance similar to the one assumed in the large-signal efficiency calculations. The various details of the selection of the resonator parameters, the measurement methods, and the cold test results, are described below.

B. Resonator Parameters

A drawing of the cold-test model of the filter-loaded output resonator is shown in Fig. 19. In view of the results of the large-signal efficiency calculations reported in the Third Quarterly Report, the resonator interacting with the beam was chosen to be a two-gap structure operating in the π mode and with a normalized gap-to-gap spacing of 2.2 radians (normalized at 5500 Mc and 140 kV). The selected filter cavity was a rectangular cavity integral with the output waveguide and operating in the TE_{101} mode. Preliminary measurements on a filter cavity of approximately the correct frequency indicated that its R/Q would be close to 190 ohms. Previous cold test measurements on a two-gap resonator like the one used had shown that its R/Q would be approximately 140 ohms (See Section III of the Third Quarterly Report). To provide some guidelines on the

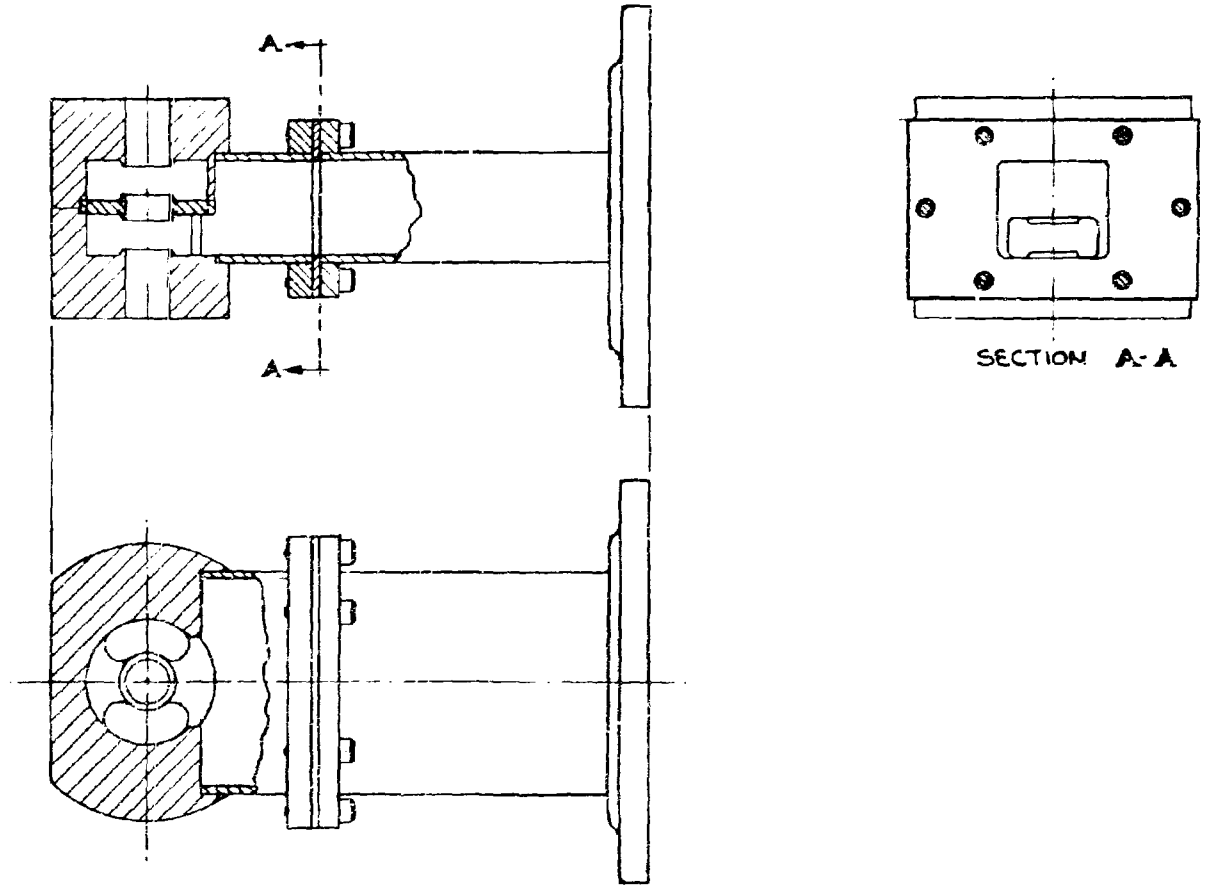

SECTION A-A

FIG. 19 COLD TEST MODEL OF THE FILTER-LOADED EXTENDED-INTERACTION OUTPUT RESONATOR

required resonant frequency and Q of the filter cavity and the π-mode frequency of the two-gap resonator, before they were coupled together, some theoretical calculations of the resonator impedance were carried out using these values of R/Q. The calculations were based on the same two-mesh equivalent circuit analysis that was used in earlier computations of filter-loaded resonator impedance.

One acceptable theoretical impedance curve is shown in Fig. 20. The resonator parameters for this case are indicated on the figure. The values listed there were used as approximate goals for the cold test cavities. It should be noted that the values specified for the frequency, Q, and R/Q of each cavity refer to the respective quantities before the filter cavity is coupled to the resonator interacting with the beam. (The Q of 2000 given for the two-gap resonator is not critical, since the Q value is so high.)

The actual parameters achieved in the cold test resonator prior to opening the coupling iris between the filter cavity and the two-gap resonator are listed below. (The Q value listed for the filter cavity is based on a Q definition in terms of half-power frequencies. This is consistent with the definition used in the two-mesh equivalent circuit analysis.) The band-center frequency goal was 5500 Mc.

Filter Cavity Parameters

Resonant frequency	5720 Mc
R/Q	195
Q	6

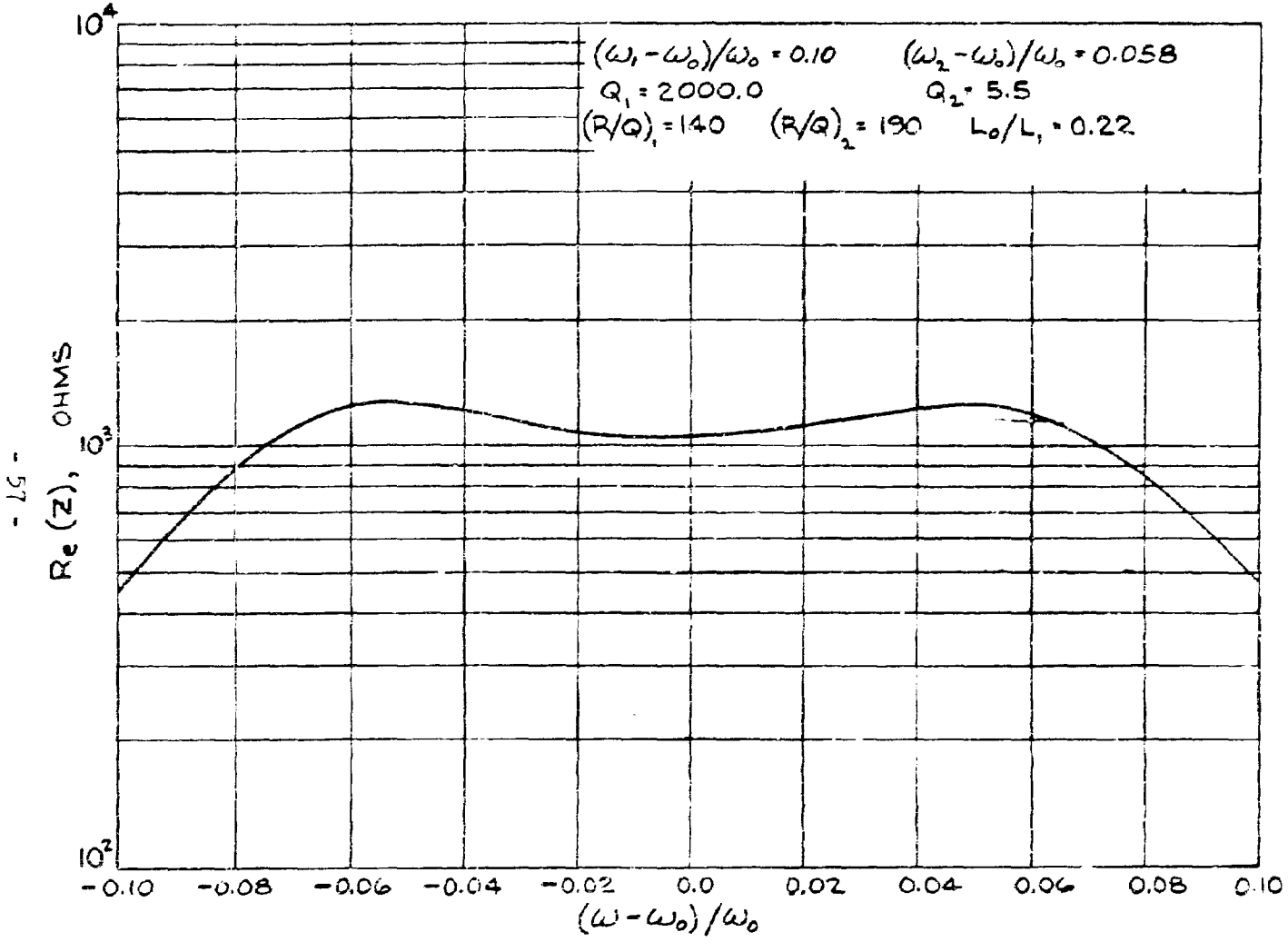

Fig. 20 - Theoretical filter-loaded output resonator interaction impedance.

Two-Gap Resonator Parameters

π-mode frequency	5925 Mc
π-mode R/Q	145
π-mode Q	3000
2π-mode frequency	7540 Mc

A comparison between these parameters and those listed on Fig. 20 shows that the two sets are close, but do not agree exactly. It was expected that some further adjustments of the cold test cavities would be necessary to obtain the desired impedance characteristics.

The coupling between the two-gap resonator and the filter cavity (represented by the parameter L_0/L_1 in the equivalent circuit) was adjusted experimentally. This was done by gradually increasing the size of the coupling iris in steps until the required bandwidth was obtained. In order to achieve the desired variation of impedance with frequency, it was also necessary to slightly adjust the Q and frequency of the filter cavity from the values listed above. The measurement procedure used to determine the resonator interaction impedance is described in Part C of this section.

The final results obtained with this cold-test resonator are displayed in Fig. 21, where the relative variation of the real part of the interaction impedance is plotted as a function of frequency. This impedance curve is quite close to the one assumed in the large-signal efficiency calculations (See Fig. 4). The cold-test curve could be further modified if desired by making additional small

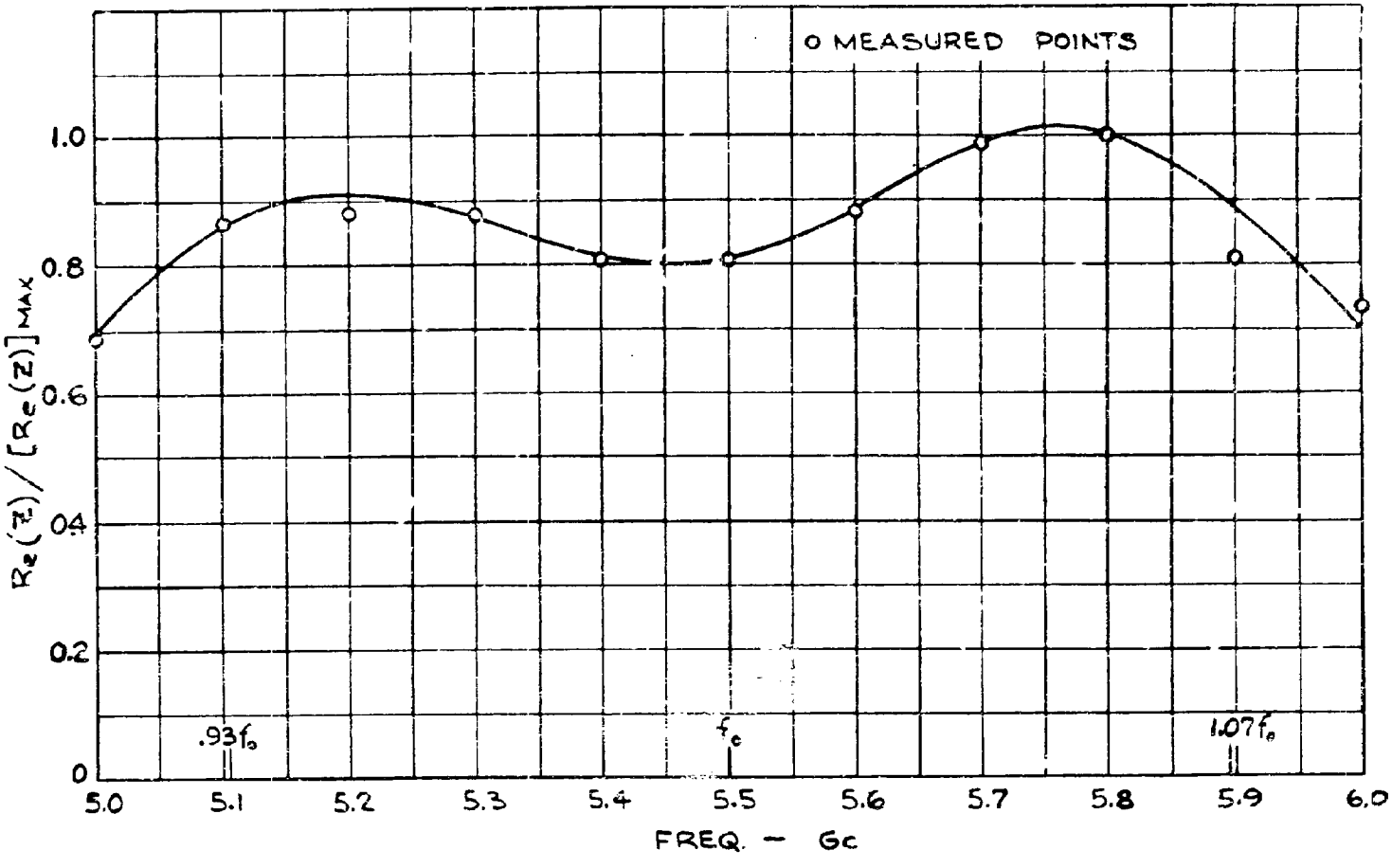

Fig. 21 - Measured variation of the real part of the interaction impedance of the cold-test resonator shown in Fig. 19.

adjustments in the resonator parameters. However, the results presented here are sufficient to show the feasibility of obtaining the desired output resonator impedance curve over a 14 percent band.

C. Measurement Methods

The basic parameters (resonant frequency, Q, R/Q) of the filter cavity and the two-gap resonator before they were coupled together were measured using conventional cold test techniques. (The measurement methods normally used on single-gap resonators can also be used on multi-gap structures providing the resonator modes are well separated, as was the case in the two-gap resonator under consideration.) The interaction impedance as a function of frequency of these individual resonators can be calculated from the measured values of Q, R/Q, and resonant frequency. Conventional cold test measurement techniques are, however, not applicable to the overall filter-loaded resonator, since the usual concepts of resonant frequency, Q, and R/Q have no meaning in this type of structure. Therefore, a new cold test method had to be developed.

The procedure used to measure the interaction impedance of the filter-loaded resonator is based on a method presented by E. Lakits[2]. In using this method, an rf signal was fed to the output waveguide of the resonator through a waveguide slotted section. At each frequency, the interaction gaps of the resonator were perturbed by inserting a small quartz rod along the axis, and the resulting change

[2] E. Lakits, "Measurement of the Interaction Impedance of a Klystron Broadband Coupling Circuit," IRE Wescon Convention Record, Session 27/2, 1961.

in the reflection coefficient phase angle was determined by a direct measurement of the shift of the standing-wave pattern. Lakits has shown that the real part of the resonator interaction impedance is proportional to the change in the reflection coefficient phase angle, providing the resonator is nearly lossless and the perturbation is small. (See Appendix A for a correction to one of his equations which, however, does not change his general conclusions.) These requirements were met in our cold test resonator by making it from copper, and by selecting the size of the quartz rod so the maximum shift in the standing-wave pattern was small compared to one-quarter of the guide wavelength. As a check on our application of the method, the relative impedance of the two-gap resonator (without the filter cavity) was measured vs. frequency using the perturbation technique. The results were compared with the impedance variation calculated from measured Q values of the resonator (determined from Q circles). This was done for two different values of Q. In both cases, the agreement between the two methods was excellent.

Lakits also describes a method for determining the phase angle of the resonator impedance but, due to a lack of time, these measurements were not made. For the same reason, no attempt was made to measure the absolute value of the interaction impedance, nor was a thorough search conducted to locate any higher-order resonator modes which might cause instability problems. At least these latter two measurements should be carried out before the resonator could be confidently built into a tube.

VI. CONCLUSIONS AND RECOMMENDATIONS FOR FUTURE WORK

A. Conclusions

During the course of this contract, we have shown the feasibility of obtaining a 14 percent 1 db bandwidth from a C-band klystron amplifier with approximately 30 db of gain and with a predicted efficiency in the range of 50 percent. The study leading to this feasibility conclusion was conducted analytically through the combined use of a small-signal computer program, described in the First Quarterly Report, and a large-signal computer program, described in the First and Second Quarterly Reports. The resonator parameters used in the final calculations were based on cold test measurements. The beam parameters assumed in the calculations were consistent with reasonable gun design.

Our study has shown that the best way to achieve the bandwidth goal without unduly sacrificing gain or efficiency is to use conventional single-gap resonators in the buncher section and a two-gap filter-loaded extended-interaction output resonator. The only element included in the final tube model which is not usually found in klystron amplifiers is the filter-loaded extended-interaction output resonator. This element of the tube was kept as simple as possible, consistent with a high efficiency level, by restricting the number of gaps in the extended-interaction resonator to two, and the number of sections in the filter load to one. Particular emphasis was placed on assuring the stability of this resonator, as well as that of the entire tube. The total number of resonators in the tube was limited to seven to keep the length as short as possible, and thus keep the

phase pushing factor to a minimum value. Higher gain could have been realized by including additional resonators in the buncher section. Calculations on the final klystron model show that it has good phase characteristics.

The 14 percent 1 db bandwidth value represents at least a 50 percent improvement over the current state-of-the-art at the 5 megawatt peak power level studied. No detailed investigation was carried out at lower peak power levels nor was CW operation studied. However, cold test results indicate that in both cases even greater bandwidth improvements may be possible. At the lower beam powers, the resonator drift-tube diameter would be smaller (for constant normalized diameter) yielding a more favorable resonator geometry and a consequent increase in the R/Q.

Calculations of the average power dissipated in the external loads of the klystron model buncher resonators showed that the maximum dissipation would be less than one kilowatt when the tube is operating at an average output power level of 70 kilowatts. The limiting factor in the average rf power output of the tube would be the heat dissipation characteristics of the drift tube section in the extended-interaction output resonator. However, this should present no serious problems, since the cold-test resonator design was similar to the design of the Eimac X-3030 output resonator, a four-gap resonator which has operated at a CW output power level of 500 kilowatts at X-band.

B. Recommendations for Future Work

From the results of this study, we have concluded that a

filter-loaded two-gap π-mode output resonator is the best choice for obtaining a wide bandwidth at a high efficiency level. The cold testing of this type of resonator should be continued. The present cold test method should be extended, or a new method developed, by which the absolute magnitude of the resonator interaction impedance can be determined. In addition, a thorough search should be made for higher order modes which might cause oscillation problems.

Extended-interaction resonators with mode overlapping should be studied. It was stated earlier in this report that conventional single-gap resonators are to be preferred over extended-interaction resonators in the klystron buncher section at the power level and frequency considered in this study. However, because of limitations in the existing theory, the investigation of extended-interaction resonators in this contract was limited to single-mode resonators. The theoretical analysis assumed that only one resonator mode is excited at a time. The cold-test resonators were deliberately constructed to have a large frequency separation between the two modes, thus assuring a minimum excitation of the non-operating mode. But the results reported in Section III-C of the First Quarterly Report indicated that there is always an appreciable excitation of the neighboring mode in a two-gap resonator even though the frequency separation between the modes is large. It follows that the simultaneous excitation of more than one mode will always be present to some extent in extended-interaction resonators and may play an important part in their behavior. It is therefore important that the effect of mode

overlapping be studied. It is possible that full use is not being made of extended-interaction resonators unless significant mode overlapping is allowed. We feel that the optimum degree of mode overlapping and the selection of optimum resonator design parameters should be determined by further analysis.

Since multi-mode operation of extended-interaction resonators has not been studied, all the possible benefits of this type of operation are not known. However, one beneficial result is immediately evident from the cold test measurements made in this contract: as the frequency separation between the resonator modes is decreased, yielding a greater amount of mode overlapping, the resonator R/Q in the π mode increases. (π-mode resonators are shown to be the best choice for both the buncher section and the output resonator in this study.) An expected benefit of utilizing more than one resonator mode is the achievement of the higher interaction impedance over a greater bandwidth. If this can be done, it is possible that the performance of a filter-loaded single-mode resonator can be matched or even exceeded by a multi-mode resonator without a filter load. The elimination of the filter cavity would greatly simplify the design of the output resonator.

GLOSSARY OF SYMBOLS

C	Equivalent cavity capacitance
d	Gap length
$\underset{\sim}{e}_3$	Unit vector for the filter cavity of Fig. 17, defined by Eq. (19)
$\underset{\sim}{e}_\pi$	π-mode unit vector, defined by Eq. (17)
$\underset{\sim}{e}_{2\pi}$	2π-mode unit vector, defined by Eq. (18)
G_c	Circuit conductance
G_e	Beam-loading conductance
i_1, i_2, i_3	RF currents circulating in the cavities of a filter-loaded resonator, defined in Fig. 17
I_1, I_2	(Section IV) Induced rf currents in the gaps of a filter-loaded resonator, defined in Fig. 17
I_1	(Sections II, III) Fundamental rf beam current
$I_\pi, I_{2\pi}$	Complex current amplitudes of the π mode and 2π mode
$\underset{\sim}{I}$	Induced rf current column vector, defined by Eq. (10)
I_o	DC beam current
I_∞	Induced rf gap current
ℓ	Axial length
L	Equivalent cavity inductance
L_0	Equivalent coupling inductance in a filter-loaded resonator (two-mesh circuit, Fig. 7, Second Quarterly Report)
L_{01}	Equivalent coupling inductance between the cavities of an extended-interaction resonator, defined in Fig. 17
L_{02}	Equivalent coupling inductance between the filter cavity and the two-gap resonator, defined in Fig. 17
n	Resonator number

p	Spacing between the centers of the gaps in an extended-interaction resonator
P_L	Power dissipated in a resonator load
Q	Total loaded Q (also called Q_L)
Q_B	Beam-loaded Q
Q_e	External Q
R	Equivalent cavity resistance
R/Q	Resonator impedance quality factor
S	Stability parameter, defined by Eq. (26)
$\underset{\sim}{\mathcal{S}}$	Column vector, defined by Eq. (59) of the First Quarterly Report
u_o	DC beam velocity
U	RF kinetic voltage
V	RF gap voltage
$\underset{\sim}{V}$	RF gap voltage column vector
V_o	DC beam voltage
V_1, V_2, V_3	Induced rf gap voltages in a filter-loaded resonator, defined in Fig. 17
V_π, $V_{2\pi}$	Complex voltage amplitudes of the π mode and 2π mode
y	Normalized axial distance ($y = \beta_e z$)
$Y_{2,1}$	Transfer admittance between two resonator gaps
$\underset{\sim}{Y}_c$	Circuit admittance matrix
Y_e	Electronic admittance (beam-loading admittance)
$\underset{\sim}{Y}_e$	Electronic admittance matrix
z	Axial coordinate
Z	Resonator shunt impedance (interaction impedance)

Z_o	Ratio of the dc beam voltage to the dc beam current
Z_{11}	Interaction impedence of filter-loaded resonator as found from the two-mesh circuit (Fig. 7, Second Quarterly Report)
$\underset{\sim}{Z}_c$	Circuit impedance matrix
Z_π	π-mode interaction impedance, defined by Eq. (20)
α	Normalized rf gap voltage magnitude ($\alpha = \lvert V \rvert / V_o$)
β_e	Propagation factor associated with the dc beam velocity ($\beta_e = \omega/u_o$)
β_q	Plasma propagation factor ($\beta_q = \omega_q/u_o$)
$\underset{\sim}{\Delta}$	Column vector defined by Eq. (60) of the First Quarterly Report
η_c	Klystron conversion efficiency
σ	(Sections II, III) Phase of the rf gap voltage
σ	(Section IV) Imaginary part of the complex frequency
ϕ	Resonator impedance phase angle
ω	Angular frequency
ω'	Real part of the complex frequency
ω_n	Angular resonant frequency of the nth resonator
ω_o	Angular frequency at the center of the band
ω_q	Reduced angular plasma frequency

APPENDIX A

DERIVATION OF A CORRECTED EQUATION USED IN THE COLD TEST PROCEDURE FOR FILTER-LOADED RESONATORS

The procedure used in this contract to determine the interaction impedance of filter-loaded resonators is based on a method suggested by E. Lakits[2]. In his method, an rf signal is fed to the output port of the resonator through a slotted section of the transmission line or waveguide. The change in the phase of the reflection coefficient looking into the output port is measured when the interaction gap(s) of the resonator is perturbed. The last equation in the second section of Lakits' paper shows that this change in the reflection coefficient phase angle is proportional to the real part of the resonator interaction impedance, providing the resonator is nearly lossless and the perturbation is small. However, there appears to be an error in the proportionality and, in addition, this equation does not follow from his preceding equations. The equation under discussion is

$$\Delta\phi = \alpha \Delta Y \qquad \text{(A-1)}$$

where

ϕ = reflection coefficient phase angle

α = real part of the resonator interaction impedance

Y = equivalent admittance of the interaction gap(s)

---

[2] E. Lakits, "Measurement of the Interaction Impedance of a Klystron Broadband Coupling Circuit," IRE Wescon Convention Record, Session 27/2, 1961.

A corrected version of this equation, which is also consistent with the earlier equations of the second section of Lakits' paper, is derived below.

The definition of the reflection coefficient ρ can be written in the form

$$\rho = \frac{Z_L - Z_o}{Z_L + Z_o} = \frac{Y_o - Y_L}{Y_o + Y_L} \qquad (A\text{-}2)$$

where

$Y_o = 1/Z_o$ = admittance of the transmission line

$Y_L = 1/Z_L$ = admittance of the load

Usually, Y_o is real and Y_L is complex. That is,

$$Y_L = G_L + j\, B_L \qquad (A\text{-}3)$$

In which case

$$\phi = \tan^{-1}\left(\frac{2\, B_L\, Y_o}{|Y_L|^2 - Y_o^2}\right) \qquad (A\text{-}4)$$

In Lakits' paper, all admittances are normalized to the admittance of the transmission line. Also, the load admittance Y_L is the admittance looking into the output port of the resonator and is denoted by Y_2. Since the resonator is assumed to be lossless, Y_2 is purely reactive. It follows that

$$Y_o = 1 \qquad (A\text{-}5)$$

$$Y_L = Y_2 = j B_2 \qquad \text{(A-6)}$$

Substituting these last two equations into Eq. (A-4), we obtain

$$\phi = \tan^{-1}\left(\frac{2B_2}{B_2^2 - 1}\right) = \tan^{-1}\left(\frac{-2j\,Y_2}{|Y_2|^2 - 1}\right) \qquad \text{(A-7)}$$

The rate of change of ϕ with respect to Y_2 may be found by differentiating Eq. (A-7). Provided the perturbation causing the change in Y_2 is small, we find

$$\Delta\phi = \frac{2j}{1 - Y_2^2}\,\Delta Y_2 \qquad \text{(A-8)}$$

In Lakits' notation, $Y_2 = C/D$, $\Delta Y_2 = \Delta Y/D^2$, $\alpha = 1/(D^2 - C^2)$, where C and D are elements of a matrix relating the rf voltage and current at the interaction gap(s) to the voltage and current at the resonator output port. Using this notation, Eq. (A-8) becomes

$$\Delta\phi = \frac{2j}{1 - C^2/D^2}\,\frac{\Delta Y}{D^2} \qquad \text{(A-9)}$$

or

$$\Delta\phi = 2j\alpha\,\Delta Y \qquad \text{(A-10)}$$

Eq. (A-10) is the corrected Eq. (A-1). If the perturbation of the interaction gap(s) is purely reactive, ΔY is imaginary and therefore $\Delta\phi$ is real.

APPENDIX B

SUPPLEMENT TO REPORT NO. ECOM-01362-4

KEY TECHNICAL PERSONNEL

Following are the key technical personnel who worked on Contract DA 28-043 AMC-01362(E) during the final period of the program. Also listed are the hours charged to the job by each individual.

Erling Lien	
Sr. Staff Research Scientist	237 hours
J. Darrell Robinson	
Sr. Development Engineer	819 hours
Marta Perry	
Mathematician	108 hours

PUBLICATIONS, REPORTS, LECTURES, AND CONFERENCES

There were no publications or reports published, or lectures presented in connection with the research performed under this contract during the period covered by this report.

There was one conference during this period. It was held at Eimac on May 3, 1966. Those attending were: Park Richmond from the U.S. Army Electronics Command, and Bill Luebke, Erling Lien, and Darrell Robinson from the High Power Microwave Tube Laboratory.

Progress on this contract during the third quarter was outlined and discussed. In addition, some of the preliminary results of the efficiency

calculations across the band with a filter-loaded output resonator were presented. It was agreed that further study should be given this type of resonator both theoretically and in cold test. The theoretical study was to include an investigation of the stability of the resonator. It was also agreed that the small-signal gain response of the buncher section should be recomputed using the latest cold test values of R/Q for the resonators.

Security Classification

DOCUMENT CONTROL DATA - R&D

(Security classification of title, body of abstract and indexing annotation must be entered when the overall report is classified)

1. ORIGINATING ACTIVITY (Corporate author)	2a. REPORT SECURITY CLASSIFICATION
EIMAC, Division of Varian San Carlos, California	Unclassified
	2b. GROUP N/A

3. REPORT TITLE

STUDY AND INVESTIGATION LEADING TO THE DESIGN OF BROADBAND HIGH POWER KLYSTRON AMPLIFIERS

4. DESCRIPTIVE NOTES *(Type of report and inclusive dates)*

Final Report - 1 March - 31 August 1966

5. AUTHOR(S) *(Last name, first name, initial)*

Lien, E.; Robinson, D.

6. REPORT DATE	7a. TOTAL NO. OF PAGES	7b. NO. OF REFS
November 1966	68	

8a. CONTRACT OR GRANT NO.	9a. ORIGINATOR'S REPORT NUMBER(S)
DA 28 043 AMC-01362 (E) b. PROJECT NO. 5024-11-905-04-78 c. d.	9b. OTHER REPORT NO(S) *(Any other numbers that may be assigned this report)* ECOM-01362-F

10. AVAILABILITY/LIMITATION NOTICES

This document is subject to special export controls and each transmittal to foreign governments or foreign nationals may be made only with prior approval of CG, USAECOM, ATTN: AMSEL-KL-TM, Fort Monmouth, New Jersey 07703.

11. SUPPLEMENTARY NOTES	12. SPONSORING MILITARY ACTIVITY
	U.S. Army Electronics Command Fort Monmouth, New Jersey AMSEL-KL-TM

13. ABSTRACT The objective of this program has been to investigate rf interaction circuits and stagger-tuning techniques leading to at least a fifty percent improvement in the 1 db bandwidth of high-power klystrons over the current state-of-the-art.

In this report, the findings of the final phase of this contract are presented. The major part of the effort during this final reporting period included: the completion of large-signal efficiency calculations across the band assuming a filter-loaded output resonator, the final theoretical design of the buncher section, theoretical stability calculations on the filter-loaded output resonator, and cold test measurements on a filter-loaded extended-interaction resonator.

The measured interaction impedance obtained with the cold-test filter-loaded output resonator closely approximated the impedance assumed in the theoretical efficiency calculations. The final buncher section, designed with the aid of the small-signal computer program, yielded a nearly constant rf drive current to the output resonator, as was assumed in the large-signal efficiency calculations. The small-signal analysis indicated that conventional single-gap resonators are to be preferred over extended-interaction resonators in the klystron buncher section at the high power level considered in this study.

The combined results of the small-signal analyses, the large-signal analyses, and the cold test measurements carried out during this contract show the feasibility of building a 5 megawatt peak-power C-band klystron amplifier with a 14 percent 1 db bandwidth, with a predicted gain of more than 30 db. The only element of the final klystron model which is not conventionally found in klystron amplifiers is the filter-loaded two-gap extended-interaction output resonator.

DD FORM 1 JAN 64 1473

Security Classification

KEY WORDS	LINK A		LINK B		LINK C	
	ROLE	WT	ROLE	WT	ROLE	WT
Broadband Klystron Extended-Interaction Cavities Double-tuned Resonator Klystron						

INSTRUCTIONS

1. ORIGINATING ACTIVITY: Enter the name and address of the contractor, subcontractor, grantee, Department of Defense activity or other organization *(corporate author)* issuing the report.

2a. REPORT SECURITY CLASSIFICATION: Enter the overall security classification of the report. Indicate whether "Restricted Data" is included. Marking is to be in accordance with appropriate security regulations.

2b. GROUP: Automatic downgrading is specified in DoD Directive 5200.10 and Armed Forces Industrial Manual. Enter the group number. Also, when applicable, show that optional markings have been used for Group 3 and Group 4 as authorized.

3. REPORT TITLE: Enter the complete report title in all capital letters. Titles in all cases should be unclassified. If a meaningful title cannot be selected without classification, show title classification in all capitals in parenthesis immediately following the title.

4. DESCRIPTIVE NOTES: If appropriate, enter the type of report, e.g., interim, progress, summary, annual, or final. Give the inclusive dates when a specific reporting period is covered.

5. AUTHOR(S): Enter the name(s) of author(s) as shown on or in the report. Enter last name, first name, middle initial. If military, show rank and branch of service. The name of the principal author is an absolute minimum requirement.

6. REPORT DATE: Enter the date of the report as day, month, year, or month, year. If more than one date appears on the report, use date of publication.

7a. TOTAL NUMBER OF PAGES: The total page count should follow normal pagination procedures, i.e., enter the number of pages containing information.

7b. NUMBER OF REFERENCES: Enter the total number of references cited in the report.

8a. CONTRACT OR GRANT NUMBER: If appropriate, enter the applicable number of the contract or grant under which the report was written.

8b, 8c, & 8d. PROJECT NUMBER: Enter the appropriate military department identification, such as project number, subproject number, system numbers, task number, etc.

9a. ORIGINATOR'S REPORT NUMBER(S): Enter the official report number by which the document will be identified and controlled by the originating activity. This number must be unique to this report.

9b. OTHER REPORT NUMBER(S): If the report has been assigned any other report numbers *(either by the originator or by the sponsor)*, also enter this number(s).

10. AVAILABILITY/LIMITATION NOTICES: Enter any limitations on further dissemination of the report other than those imposed by security classification, using standard statements such as:

(1) "Qualified requesters may obtain copies of this report from DDC."

(2) "Foreign announcement and dissemination of this report by DDC is not authorized."

(3) "U. S. Government agencies may obtain copies of this report directly from DDC. Other qualified DDC users shall request through

_____."

(4) "U. S. military agencies may obtain copies of this report directly from DDC. Other qualified users shall request through

_____."

(5) "All distribution of this report is controlled. Qualified DDC users shall request through

_____."

If the report has been furnished to the Office of Technical Services, Department of Commerce, for sale to the public, indicate this fact and enter the price, if known.

11. SUPPLEMENTARY NOTES: Use for additional explanatory notes.

12. SPONSORING MILITARY ACTIVITY: Enter the name of the departmental project office or laboratory sponsoring *(paying for)* the research and development. Include address.

13. ABSTRACT: Enter an abstract giving a brief and factual summary of the document indicative of the report, even though it may also appear elsewhere in the body of the technical report. If additional space is required, a continuation sheet shall be attached.

It is highly desirable that the abstract of classified reports be unclassified. Each paragraph of the abstract shall end with an indication of the military security classification of the information in the paragraph, represented as *(TS)*, *(S)*, *(C)*, or *(U)*.

There is no limitation on the length of the abstract. However, the suggested length is from 150 to 225 words.

14. KEY WORDS: Key words are technically meaningful terms or short phrases that characterize a report and may be used as index entries for cataloging the report. Key words must be selected so that no security classification is required. Identifiers, such as equipment model designation, trade name, military project code name, geographic location, may be used as key words but will be followed by an indication of technical context. The assignment of links, rules, and weights is optional.